Sustainable Materials and Technologies 41 (2024) e01001

Contents lists available at ScienceDirect

Sustainable Materials and Technologies

journal homepage: www.elsevier.com/locate/susmat

Environmentally friendly calcium carbonate-polydopamine microcapsules with superior mechanical, barrier, and adhesive properties

Daniele Baiocco [a], Benjamin T. Lobel [b], Mohammed Al-Sharabi [c], Olivier J. Cayre [b], Alexander F. Routh [c], Zhibing Zhang [a,*]

[a] School of Chemical Engineering, University of Birmingham, Birmingham, UK
[b] School of Chemical and Process Engineering, University of Leeds, Leeds LS2 9JT, UK
[c] Department of Chemical Engineering and Biotechnology, University of Cambridge, Cambridge CB3 0AS, UK

ARTICLE INFO

Keywords:
Green microencapsulation
Bio-inspired
Sustainability
Bio-adhesion
Micromanipulation

ABSTRACT

There is a rising need to deliver perfume molecules to fabric surfaces during washing cycles to enhance consumers' perception. With upcoming regulations phasing out intentionally produced microplastics by 2027, the focus is on sustainable alternatives to conventional non-biodegradable synthetic microcapsules (e.g. melamine-formaldehyde). Calcium carbonate ($CaCO_3$) has shown promise to form the microcapsule shells due to its environmental benignity, inexpensiveness, and potential for liquid formulations, particularly detergents. Notwithstanding, its inherent porosity undermines the performance of the ensuing microcapsules. Bio-inspired by the adhesive properties of mussel proteins, dopamine is proposed for forming a protective organic coating on $CaCO_3$-based microcapsules. This research aims towards developing primary microcapsules with $CaCO_3$ shells encapsulating hexylsalicylate (HS) as a perfume oil, applying a polydopamine (PDA) coating via oxidative auto-polymerisation of dopamine-hydrochloride (pH 8.5), and conducting a comprehensive analysis of morphological, mechanical, barrier, and adhesive properties through advanced techniques, namely fluorescent-sensing/scanning electron microscopy (SEM), micromanipulation, UV–Vis spectrometry, and a microfluidic chamber fitted with polyethylene-terephthalate (PET) fabrics. The obtained microcapsules ($D_{[3,\ 2]}$=31.2 ± 0.4 μm) exhibited a spherical core-shell structure with a smooth PDA-coated surface. Mechanical assessments reveal remarkable rupture stress (2.2 ± 0.3 MPa) comparable to that of commercial microcapsules. After one month in water, ~40% of HS was released from PDA-coated microcapsules, while the primary ones released the entire amount within 4 h. When mimicking washing conditions (pH 9), the PDA-coated microcapsules demonstrated improved retention (~60%) on the PET substrate at hydrodynamic shear stress of ~1 Pa, whereas that of the primary microcapsules was below 10%. Overall, this study suggests the successful fabrication of eco-friendly microcapsules featuring a hybrid inorganic-organic shell, with enhanced mechanical strength, reduced leakage, and improved adhesion, showcasing their potential in applications within the fast-moving consumer goods industry.

1. Introduction

Within microencapsulation, modifying surfaces and shell materials into suitable architectures to achieve specific properties is rapidly advancing [1,2]. To this end, microcapsules designed to exhibit e.g. mechanical robustness and hydrophobicity/hydrophilicity can provide additional desirable functionalities, such as chemical selectivity, electrothermal isolation, controllable permeability, and enhanced adhesiveness via forming an outer coating onto a template or primary microcapsule [3,4]. Thus, polymeric/nonpolymeric surface modifying agents (SMA) are extensively employed, providing clear-cut advantages for the performance of microcapsules in their end-use [2,5]. Indeed, SMA-coated microcapsules can rupture to deliver their payload onto a desired substrate to fulfil the desired function upon exposure to extraneous stimuli (e.g. mechanical action, pH, and temperature) [3]. SMA-coated microcapsules have become popular for detergents, paints, and many other sustained release applications. As described by Li et al. [6] the surface of aliphatic poly(urea) (PU) microcapsules can be modified with acetoacetyl functional polyelectrolytes to tether the amino groups to the PU matrix thereby achieving a strong covalent decoration, which

* Corresponding author.
E-mail address: z.zhang@bham.ac.uk (Z. Zhang).

https://doi.org/10.1016/j.susmat.2024.e01001
Received 23 January 2024; Received in revised form 10 May 2024; Accepted 31 May 2024
Available online 7 June 2024

may lead to their improved adhesiveness onto several synthetic substrates.

In literature, self-healing poly(urea formaldehyde) (PUF) microcapsules were fabricated via in-situ polymerisation and their surface was then modified by grafting a silane coupling agent (3-amino-propyltriethoxysilane (KH550)) [7]. It has been demonstrated that a KH550 layer as the outermost surface of PUF microcapsules may enhance their interfacial adhesion performance onto epoxy resin compounds. In addition, Katoueizadeh et al. [8] have provided a morphological study on the surface modification of PUF microcapsules using the same silane coupling agent. KH550 was capable of binding firmly onto a microcapsule surface, thereby increasing its roughness. Such functionalisation was effective for improving the thermal properties of microcapsules, as well as enhancing their interfacial adhesion onto required epoxy matrix, which is crucial for a broad spectrum of applications.

Similarly, the surface of linseed oil laden microcapsules with a poly (methyl methacrylate) (PMMA) shell was functionalised with hexamethylene diamine (HDMA) by Navarchian et al. [9] in order to maximise the interfacial adhesion between the PMMA shell and an epoxy matrix. This was for industrial paint and coating systems.

Ong et al. [10] have reported the surface modification of commercially available microcapsules with a 90% octadecane payload as phase change material (PCM) surrounded by a polymeric shell. Polyurethane acrylic was employed as a SMA to lacquer the polymeric shell homogeneously in order to act as an adhesive agent for additives (metal nanotubes) to be coated uniformly onto the shell, for an increased thermal conductivity.

Additionally, commercial PCM microcapsules with a melamine-formaldehyde (MF) shell were functionalised with polypyrrole [11]. Interestingly, it was reported that PCM microcapsules containing $<2\%$ (*w*/w) polypyrrole possessed a significantly higher energy storage/conversion performance, which can be beneficial to a plethora of applications, such as photothermally sensitive textiles.

Microcapsule adhesiveness is imperative in a wide range of industrial applications. If the adhesion is too weak, the microcapsule may detach from the target surface, leading to a loss of the encapsulated substance or functionality. Therefore, it is crucial to enhance the adhesion of microcapsules by SMA or dual coatings to achieve the desired stability for a specific application (e.g. adhesion of microcapsules to mucosal membranes in pharmaceutics, edible matrices in food and beverages, fabrics in laundry process) [12].

In literature, the fabrication of dually coated microcapsules has been reported, with particular emphasis on fully synthetic (PU [13]) and hybrid systems (organic-inorganic composites e.g. MF-$CaCO_3$ [3]) via interfacial polymerisation (IP) on oil-in-water emulsion droplets, a technique which is only suitable for a limited set of synthetic polymers [12,14]. Moreover, many SMA as well as shell−/template-forming ingredients are shrouded in controversy due to their partial/full synthetic nature and poor biodegradability [12,15]. Although a challenging task, it has become essential to reformulate commercial microcapsules without diminishing their performance to overcome the use of plastics and unsafe shell chemicals (e.g. formaldehyde) in favour of biocompatible, completely biodegradable, inexpensive, easily processed, environmentally conscious and consumer friendly materials [16]. Recently, worthwhile endeavours have been undertaken by several research groups towards tackling some of the current challenges in microencapsulation leading to novel dually coated microcapsules with robust shells from natural biopolymers. Yu et al. [17] have combined gelatine and gum Arabic (GA) via coacervation on emulsified fish oil droplets resulting in primary microcapsules which were subsequently atomised in the presence of maltodextrin as a shell strengthening agent. As reported, their measured rupture force (1.8 ± 0.3 mN; size 15.9 ± 1.4 μm) was statistically comparable to that of commercial MF microcapsules (2.1 ± 0.3 mN; size ~14 μm) [17]. Similarly, Baiocco et al. [4] employed plant-based biopolymers (fungal chitosan and gum Arabic) to fabricate a primary shell around peppermint oil droplets via coacervation, followed by the deposition of a secondary maltodextrin coating by spray drying, which yielded functionalised dual shell microcapsules with a spherical shape. In addition, inorganic materials, such as silicates, phosphates, and carbonates may form mechanically strong microcapsule shells [18]. Indeed, $CaCO_3$ is environmentally benign and potentially biocompatible [19], and has been proven suitable for building microcapsules with robust walls inexpensively, thereby enabling the release of the active material facilely and on-demand by pH variation [3]. Notwithstanding, these inorganic materials typically exhibit significant inherent porosity, which is a disadvantage for the retention of small molecules. Therefore, additional coatings are required to be built on top of $CaCO_3$ to form composite architectures capable of retaining the encapsulated active for longer [12]. Indeed, highly performant plastic materials should be avoided in favour of safe and degradable biopolymers. Other than gum Arabic, chitosan, and gelatine, another microencapsulation-suitable material is dopamine that has been exploited in its polymerised form, polydopamine (PDA), in combination with other ingredients [1]. Inspired by the excellent bio-adhesiveness of mussel proteins (i.e. catecholamine), PDA is a promising catecholamine biopolymer that may form homogeneous films on many substrates [20]. Kang et al. [21] have built a protective PDA coating onto polystyrene, and polyurethane-urea formaldehyde as a shell of microcapsules [21], which are microplastic materials and hence not environmentally acceptable. Similarly, Wang et al. [1] have built bioadhesive PDA films onto primary polystyrene microcapsules via oxidative self-polymerisation of PDA, with a potential for biomedical applications (sustained release of human bone morphogenetic protein-2 (BMP-2)). As reported, PDA was effective as a SMA resulting in functionalised microcapsules with an increased surface adhesiveness, hence a higher BMP-2 surface adsorbability. Furthermore, PDA has demonstrated biocompatibility with numerous biological tissues, preserving their phenotypic integrity, holding promise for medical treatments [22,23]. Other than therapeutic applications, PDA was proven suitable for tethering onto essential oil emulsion droplets which had been stabilised with cinnamoylchloride-treated cellulose nanocrystals, with a potential for the encapsulation of insecticides [24]. Also, Zou et al. [25] have fabricated PDA-layered microcapsules via oxidative auto-polymerisation of monomeric dopamine to act as a SMA for the controlled release of hydrophobic pesticides (i.e. λ-cyhalothrin). As documented by Wang and Lv [26], an ultrathin PDA shell (50 nm) with a hierarchical structure can be attained around a metal organic framework (MOF) as the template, which may be beneficial for the confinement of enzymes. Generally, PDA films as the outermost layers of microcapsules have proven conducive to diminishing the leakage of costly actives. Such microcapsules adhere to many substrates, such as cuttings of polyethylene (PE) and polyethylene terephthalate (PET) bottles [27], regardless of their smooth/porous/rippled nature, as well as aromatic polyester fibres due to the hydrogen bonding and indolic/catecholic $\pi - \pi$ stacking [21]. As a step forward, Li et al. [28] have produced soft PDA microcapsules for insulin delivery using a simple and cost-effective technique. This was accomplished via the auto-oxidative assembly of PDA onto sacrificial templates (manganese carbonate). These structures were chemically removed upon PDA formation, which likely affects the mechanical properties, structural stability, and durability of the microcapsules. Moreover, no systematic information on the mechanical performance of these microcapsules has been explicitly reported. Although claims for PDA as a fully biodegradable material are encountered in literature, very little is known on its potential biodegradability and mechanism thereof, which remains to be investigated [29,30]. In the light of the above, the present study aims to evaluate the feasibility of depositing an outer coating of PDA onto primary $CaCO_3$-shell microcapsules, to enhance their performance properties, namely, mechanical strength, and storage stability. Moreover, the adhesion capability of the ensuing hybrid (inorganic-organic) microcapsules onto commercially equivalent PET substrates was investigated in comparison with that of primary microcapsules using an advanced microfluidic setup [12]. Our findings suggested that the hybrid inorganic-organic architectures may

provide a new route to control the mechanical, barrier and surface properties of microcapsules that increased their interfacial adhesion to PET substrates, towards more user and environmentally friendly formulations with natural and bio-inspired materials.

2. Materials & methods

2.1. Materials

Calcium chloride ($CaCl_2$) anhydrous flakes (CAS 7440-70-2) were obtained from SLS (Scientific Laboratory Supplies, Nottingham, UK), which were manually ground into a fine powder using an agate mortar and pestle with a diameter of 70 mm. Anhydrous sodium carbonate (Na_2CO_3; CAS 497–19-8) and sodium tetraborate ($Na_2B_4O_7$; CAS 1330-43-4) buffer tablets (pH 9.2; make-up volume = 0.1 L/tablet) were supplied by Fisher Scientific (Loughborough, UK). Dopamine hydrochloride ($C_8H_{11}NO_2$·HCl; CAS 62–31-7) was bought from Alfa Aesar (Heysham, Lancashire, UK). Pristine calcium carbonate ($CaCO_3$) nanoparticles (NPs; 20–40 nm) were obtained from SkySpring Nanomaterials, Inc. (Houston, TX, US). Hexylsalicylate (>99.0%, specific density 1040 kg·m^{-3}) as the model oil, Nile Red (NR; CAS 7385-67-3) as the fluorescence sensing dye, sorbitan trioleate (Span 85; CAS 26266–58-0) and polyoxyethylene sorbitan monolaurate (Tween 20; CAS 9005-64-5) as the emulsifiers, fuming hydrochloric acid (HCl; 36% *w/v*; CAS 7647-01-0) and sodium hydroxide (NaOH, CAS 1310-73-2) as pH adjusters, 1-propanol (PrOH; CAS 71–23-8) as the blank and receptor medium for UV–Vis analysis, ethylene-diaminetetraacetic acid (EDTA; CAS 60–00-4), sodium bicarbonate ($NaHCO_3$; CAS 144–55-8), and ethanol (CAS 64–17-5) were purchased from Merck (Gillingham, Dorset, UK). All the chemicals were of analytical grade and stored by following the Safety Data Sheet (SDS) guidelines and utilised without further purification. All solutions were prepared using Milli-Q water (18.2 MΩ·cm^{-1} at 25 °C).

2.2. Primary encapsulation via double emulsion ($w_1/o/w_2$)

A primary water phase (w_1 = 15 mL) was prepared to obtain a solution of Na_2CO_3 at 2.5 M (below its saturation point at 25 °C, 2.7 M [31]) to allow the complete dissociation of the salt in water ($Na_2CO_{3(s)} \rightarrow 2\,Na^+_{(aq)} + CO^{2-}_{3(aq)}$). Tween 20 (0.015 g) as a hydrophilic emulsifier was instilled to w_1 (0.1% *w/v*) under magnetic stirring over 10 min. Subsequently, w_1 was transferred into a double-glazed jacketed vessel (J_1, capacity 100 mL, working diameter 38 mm) connected to a water circulating bath (Grant LT EcoCool 100, Grant Instruments Ltd., Cambridge, UK) operating at 25.0 ± 0.2 °C. An oil phase (o_{HS}) was prepared in a separate beaker employing HS (30.0 g) as the model ester oil which possesses low water solubility (~10 mg/L at ~20 °C) [16]. NR (<0.5 mg) as the fluorescent sensing dye and Span 85 (0.3 g) as a hydrophobic emulsifier were added to o_{HS} and left to stir magnetically until their complete dissolution. A primary water-in-oil (w_1/o_{HS}) emulsion (w_1-to-o_{HS} weight ratio 1:2) was generated in J_1 by instilling w_1 into o_{HS} under stirring using an overhead stirrer (IKA Eurostar 20, Germany, EU) paired with a six-blade Rushton turbine (Ø 34 mm; blade dimension 1.5 × 0.75 cm) running at 1500 rpm over 15 min (Fig. 1- step 1).

A second water phase (w_2 = 100 mL) was prepared in another double-glazed jacketed reactor (J_2, capacity 500 mL, working diameter 79 mm) connected to a programmable temperature-controlled water circulating bath (Dyneo DD300F, Julabo UK Ltd., Stamford, UK). Pristine $CaCO_3$ NPs (5 g) were added to w_2 under vigorous stirring (IKA 2) to form a well dispersed suspension. Tween 20 (0.01 g) (Tween 80-to-w_2 weight ratio 1:100) was added to the continuous phase (w_2) and stirred (400 rpm over 5 min) at which point a mild froth at the air-w_2 interface was formed due to air entrained into pockets within the water phase whilst stirring continuously. Thus, ~0.2 mL of 1-octanol as a defoaming agent was spread over the air-w_2 interface to eliminate any frothing.

Subsequently, the primary w_1/o emulsion was withdrawn and gradually mixed with w_2 into J_2 whilst stirring with a Rushton turbine (1050 rpm; 15 min) at 25.0 ± 0.2 °C in order to generate a non-reactive double emulsion ($w_1/o/w_2$) (Fig. 1- step 2). The experimental setup included a stainless steel four baffles to stimulate mixing (baffle dimensions: length × width × thickness 10 × 0.75 × 0.1 cm). The stability of the double emulsion was preliminarily inspected by optical microscopy (Leica DMRBE, Leica, Wetzlar, Germany, EU). In addition, the mean size of the resulting droplets was analysed via open-source image analysis software (ImageJ 1.53c, National Institute of Health, Bethesda, MD, USA).

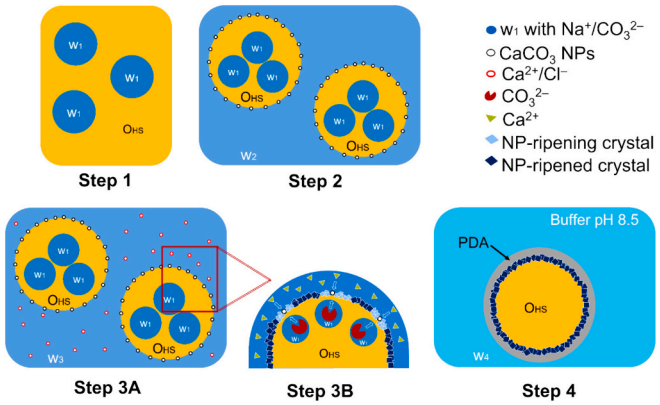

Fig. 1. Schematic depiction of the mechanism of fabricating hybrid $CaCO_3$-PDA based microcapsules with a core of HS via double emulsion ($w_1/o/(w_2 + w_3)$ – step 1,2) and interfacial crystal ripening of $CaCO_3$ (primary encapsulation; step 3 A,B) followed by the deposition of a PDA coating (secondary encapsulation; step 4).

A tertiary aqueous phase (w_3 = 100 mL) containing 1.0 M $CaCl_2$ and 0.05 g of Tween 20 was prepared in a separate beaker ($CaCl_{2(s)} \rightarrow Ca^{2+}_{(aq)} + 2Cl^-_{(aq)}$). A volume of 75 mL of w_3 was loaded onto a 150-mL disposable sterile plastic syringe (Becton Dickinson S.A., Spain, EU) and mounted onto a motorised syringe pump infusing system (PHD Ultra, Harvard Apparatus, Holliston, MA, US) connected to J_2 (liquid height (H)/Tank diameter (T) = 1; T = H = 0.15 m; Clearance (C)/Impeller Diameter (D) ~ 0.75; thermostated at 25.0 ± 0.2 °C) using soft platinum-cured silicone tubing (inner diameter 2.8 mm; Masterflex L/S, Cole-Parmer Instrument *Co.*, Vernon Hills, IL, USA). The flowrate (250 μL/min) was initiated to induce the ionic exchange reaction between CO_3^{2-} (diffusing through the oil phase) and Ca^{2+} (diffusion through the continuous bulk phase) for the ions to meet at the $o_{HS}/(w_2 + w_3)$ interface (Fig. 1-step 3 A) over 5 h. An excess of Ca^{2+} was instilled into the system (Ca^{2+}/CO_3^{2-} weight ratio ≃ 2) at pH 8.2 (pH meter FP20, Mettler Toledo, Leicester, UK). The interfacial mechanism of crystal ripening is depicted in Fig. 1-step3B) The gradual ripening of $CaCO_3$ crystals to form the microcapsule walls around the oil droplets was inspected by optical microscopy.

2.3. Secondary encapsulation

The hybrid double shell microcapsules were prepared from the primary microcapsules using dopamine hydrochloride (monomer) onto the ripened $CaCO_3$ shells being used as templates. An aliquot of the primary microcapsule suspension (0.6 g) was withdrawn and transferred into a vessel containing a sodium tetraborate (1 M) buffer solution (11 mL) at pH 9 and room temperature. Adjustments to pH 8.5 were carried out using drops of HCl_{aq}. This pH is required to facilitate the oxidation of dopamine in the presence of oxygen dissolved in water [32]. The monomer (42.5 mg) was carefully added into the buffer resulting in a dopamine concentration of 3.5 g·L^{-1}. The concentration of dopamine must be higher than 2 g·L^{-1} to enable its deposition onto the template other than forming in bulk [32]. However, a concentration of dopamine

>5 g·L^{-1} should be avoided due to the limited supply of oxygen in water (limited reactant). The oxidative auto-polymerisation was continued for 24 h under continuous magnetic stirring to enable the deposition of polydopamine (PDA) onto the inorganic ($CaCO_3$) template (Fig. 1- step 4), which is facilitated at alkaline pH 8.5 [33].

2.4. Characterisation: analytical techniques

2.4.1. Bright-field optical and fluorescence sensing microscopy

Real-time images of double emulsion $w_1/o/(w_2 + w_3)$ droplets as well as the resulting primary/secondary microcapsules were captured via a bright field optical microscope with a digital camera (Motic Pro 252, Wetzlar, Germany, EU) using PL Fluotar 5×/0.12 and 10×/0.30 objective lenses. For the detection of fluorescence sensing molecules (i.e. NR-dyed HS), a blue illumination emitting source at the operational wavelength of 460 nm was applied with a cool-LED pE-300 fluorescence filter. A H3 filter block cube (BP420–490) with a suppression filter (LP 515) and a dichromatic light-splitting mirror (510) were applied to the designated configuration to exploit the highest possible image resolution and field planarity.

2.4.2. Scanning electron microscopy (SEM)

Scanning electron microscopy (SEM) was employed to observe the morphology and surface topography of microcapsules via a benchtop SEM microscope (magnification range: 15–30,000×, Hitachi TM3030, Hitachi HighTech, Japan) equipped with high resistivity Energy Dispersive X-ray (EDX) silicon drift detectors (SDD) for elemental microanalysis (Bruker Quantax 70, Bruker Corporation, Billerica, MA, USA). The microscope was operated under high vacuum mode ($<10^{-3}$ Pa) and 15 kV of accelerating voltage. Images were generated under backscattered electron (BSE) detection mode with an integrated four-segment detector. An aliquot (~100 μL) of microcapsule suspension was transferred onto an aluminium pin stub coated with two-side adhesive carbon tape. The sample was processed for platinum sputtering under high vacuum ($<10^{-2}$ Pa) prior to SEM imaging (Polaron Sputter Coater SC7640, QuorumTech, Sussex, UK) to achieve a ~ 8 nm thick conductive layer.

2.4.3. Particle sizing

Particle sizing of both primary and secondary microcapsules was undertaken with laser diffraction via a He—Ne laser beam detector capable of detecting particles in a size range of 50 nm – 1 mm (Mastersizer 2000, Malvern Instruments Ltd., Malvern, UK). Briefly, an aliquot (~5 mL) of microcapsule suspension was transferred into the continuously stirred dispersing unit (2000 rpm) preloaded with deionised water (~120 mL). The analysis was carried out using the required refractive indices ($RI_{CaCO3} \sim 1.589$; $RI_{PDA} \sim 1.491$; $RI_{water} \sim 1.334$). The Sauter diameter ($D_{[2,\ 3]}$) was calculated as the average of five consecutive measurements.

2.4.4. Encapsulation efficiency and payload

The encapsulation efficiency and payload of microcapsules were quantified by UV–Vis spectrophotometry using a single standard method (i.e. 36% (*v*/v) PrOH as the blank). A small amount of microcapsule slurry (50 mg) was suspended in 36% (*v*/v) PrOH as the receptor medium (20 mL) within airtight vials which were then left under ultrasonication for 2 h (VWR International Ltd., USC100TH, Lutterworth, UK). The receptor medium was acidified to pH ~ 3 using $HCl_{(aq)}$. The acidification allowed the dissolution of $CaCO_3$ (primary microcapsules) whereas the ultrasonication allowed the complete breakage of the microcapsule shells (hybrid microcapsules) to release HS into 36% (v/v) PrOH. The solubility of HS into 36% (v/v) PrOH was found to be >15 kg·m^{-3} according to Mercade-Prieto et al. [34]. The insoluble polymeric debris was removed via centrifugation (2000 ×*g*; 5 min). The supernatant (1 mL) was analysed on UV–Vis (2021 CE, Cecil Instruments Ltd., UK) at its maximum absorption wavelength (306 nm).

2.4.5. Release studies

The oil leakage from microcapsules was investigated as per our previous work [16]. Briefly, 20 mg of microcapsule slurry was contained into a dialysis membrane that had been pre-cut to 5 cm length (wet diameter 21.3 mm, 0.36 mL·mm^{-1}, molecular weight cut-off 14 kDa, BioDesign Dialysis Tubing™, D004, BioDesign Inc. of New York, NY, US). The membrane was pre-treated to remove glycerol and other pollutants (sulphides, heavy metals, etc.) possibly occurring on its surfaces. The membrane was immersed into an aqueous solution containing EDTA (12 mM) and $NaHCO_3$ (2.5% (*w*/w)) which was boiled for 15 min. Tap water was run to cleanse off glycerol for 2.5 h followed by a thorough rinse-off using demineralised water. Each membrane was loaded with 2 mL of demineralised water at pH 9, folded twice, and pegged on at either end securely. The membrane was immersed into the desired receptor medium (i.e. 100 mL demineralised water pH 9) and magnetically stirred at ambient temperature (22 ± 1 °C). Oil leakage was monitored over time by UV–Vis sampling (306 nm) an aliquot (1 mL) from the receptor medium into a quartz cuvette (10 mm path length, Hellma UK Ltd., Essex, UK) at specific intervals. Each withdrawal was followed by adding 1 mL of fresh demineralised water into the testing receptor medium to assure the maintenance of sink conditions effectively.

2.4.6. Micromanipulation

The microcapsules were assayed for their mechanical properties by a micromanipulation technique using a self-built apparatus [35] coupled with a side-view high speed camera (4912–5010/000, Cohu, CA, US). An output glass tube with a finely polished flat-end tip (~50 μm) was attached to a force transducer (403 A 1,529,011, executable sensitivity 0.4939 mN·V^{-1}). Two droplets (~0.15 mL) of a diluted microcapsule suspension were placed onto a pre-cut glass slide (~2.5 cm^2; thickness ~ 1 mm). Subsequently, the glass slide was fixed onto the rig stage. Thirty individual microcapsules were squashed at a compression speed of 2.0 μm·s^{-1}. The response generated was processed to calculate the corresponding force versus displacement for each microcapsule. The system compliance was calibrated three times to calculate the actual distance travelled by the force probe (displacement) when rupturing each microcapsule [36].

2.4.7. Adhesiveness

The adhesive properties of both primary and hybrid microcapsules were analysed according to our previous work [12]. Briefly, a microfluidic flow chamber device was fitted with a flat and transparent PET film (thickness 0.25 ± 0.05 mm; Goodfellow Cambridge Ltd., Huntingdon, UK) as the microcapsule substrate. The chamber was inoculated with a diluted microcapsule suspension (0.25% *w*/w; pH 9). Increasingly high hydrodynamic shear stresses (0–4 Pa) were operated by feeding the aqueous solution at pH 9 via a motorised infusion pump (corresponding flowrate range 0–50 mL·min^{-1}). The retention of primary/hybrid microcapsules was real-time monitored by optical microscopy and further quantified by ImageJ analysis (ImageJ 1.53 t, National Institutes of Health (NIH), US), which represents their adhesiveness to the substrate.

3. Results and discussion

3.1. Double emulsion to primary microcapsules

Bright field optical microscopy has been utilised as a preliminary screening tool to investigate size, morphology, and coalescence tendency of emulsion droplets. Fig. 2 A1 displays an ensemble of double emulsified ($w_1/o/w_2$) droplets with a spherical shape. As can be seen, a monolayer of individual droplets is visible where each possesses a clear and dark outline at its oil-water (o/w_2) interface after emulsification (15 min). This is likely due to the combined effect of the emulsifying agents (Tween-Span) and $CaCO_3$ nanoparticles being adsorbed at the oil-water interface, as also visible under fluorescence (Fig. 2 A2). The effectiveness of a single emulsifier/blend of emulsifiers depends on its

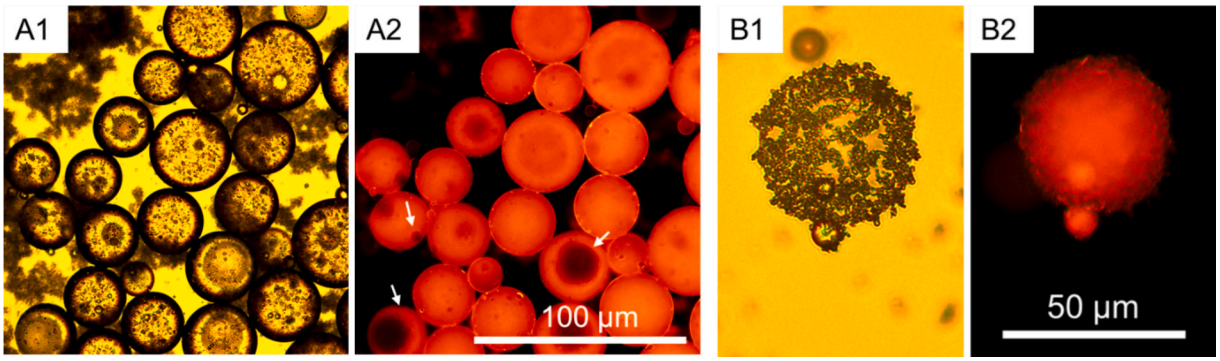

Fig. 2. Optical (A1, B1) and fluorescence sensing (A2, B2) micrographs of double emulsions (A1, A2) and crystal ripening via Pickering emulsion on $CaCO_3$ NPs as templates (B1, B2) after 4 h. Conditions: a primary emulsion was generated by instilling a primary water phase (w_1 containing CO_3^{2-} ions) into the oil (HS) phase (o_{HS}) under continuous stirring. The primary emulsion was mixed with a secondary water phase (w_2) containing pristine $CaCO_3$ NPs, thereby generating a non-reactive double emulsion ($w_1/o_{HS}/w_2$) (A1). A tertiary water phase (w_3 containing Ca^{2+} ions) was gradually inoculated to induce the interfacial self-assembly of $CaCO_3$ crystals (B1).

capability of adsorbing rapidly at the interface to lower the interfacial tension [37]. It is crucial for an emulsifier to generate a protective film around the droplets homogeneously, hampering prompt coalescence. Therefore, the type of emulsifier should be selected in accordance with this requirement. As reported in our previous studies, large compatibility between ester oils (HS) and sorbitan trioleate–polyoxyethylene sorbitan monolaurate systems was proven [15]. Interestingly, there appeared to be a good stability of emulsified HS droplets over an extended period of time up to six hours. Other than a net decrease of the interfacial energy, this was possibly due to a positive increase of the surface (visco)elasticity of droplets [38]. Similar effects are also observed with other low molecular weight emulsifiers such as lecithin, mono- and diglycerides [39], which may enable the droplets to stretch away in bulk without being permanently deformed and subsequently coalesced. To this end, solid, pristine, spherical $CaCO_3$ nanoparticles were used, in combination with the liquid emulsifiers referred to above, to promote the steric stabilisation of HS droplets in the aqueous bulk phase. According to Bai et al. [40], the network of relatively highly charged NPs is primarily effective for decreasing the interfacial energy directly, thereby stabilising o/w emulsions. Although the whole stabilisation mechanism of Pickering emulsion is not yet fully understood, NPs are also speculated to improve the interfacial wettability of (super) hydrophobic phases [41] which may possibly promote a higher electrosteric activity at the interface, hence stronger and longer lasting stabilisation. As suggested by Asare-Asher et al., when (nano)particles are adsorbed onto the surface of a liquid droplet (i.e. hydrophobic phase), its surface elasticity is ameliorated by the presence of the liquid menisci between the solid NPs [42]. Indeed, Powell and Chauhan reported that the surface elasticity of a Pickering oil-water interface depends on its surface coverage, and hence on the interfacial distribution of the liquid menisci among the (nano)particles [38]. Similar findings were corroborated by Frost and coworkers in the presence of (nano) particle-stabilised oil-in-aqueous liquid emulsion droplets [43]. The authors observed that meniscus-meniscus interactions between the NPs can be modulated by adjusting the wettability of the particles, which might improve the surface elasticity of the droplet.

As shown herein (Fig. 2), the Pickering emulsions generated using $CaCO_3$ NPs assisted by the emulsifiers have proven suitable against oiling off, creaming, and coalescence, thereby yielding kinetically stable o/w_2 droplets at least during the required timeframe prior to microencapsulation [15,40]. Besides interfacial stabilisation, $CaCO_3$ NPs may participate in the microencapsulation process in other ways, such as nucleation kernels for the mineralisation of $CaCO_3$ walls (by $CaCl_{2(aq)}$ addition) to encapsulate the HS droplets individually. Fig. 2B1 shows the formation of $CaCO_3$ crystals via o/w interfacial crystallisation, which seemed to form a relatively dense inorganic scaffolding around the hydrophobic droplet. The mineralisation advancement to form the inorganic shell and the kinetics of the ionically driven reaction between CO_3^{2-} and Ca^{2+} can be controlled by tuning the addition of $CaCl_{2(aq)}$ at a moderate flowrate (250 μL/min). This would allow Ca^{2+} (dispensed in the aqueous bulk phase) to meet CO_3^{2-} (occurring in w_1) at the $o/(w_2 + w_3)$ interface. As can be seen in Fig. 2A1, multiple w_1 microdroplets in the range of ~0.5–3 μm containing CO_3^{2-} ions were individually entrapped within the hydrophobic phase (o). The size of the outer droplets was analysed by ImageJ yielding 30.1 ± 1.4 μm. The typical droplet-in-droplet configuration was also evident under fluorescence sensing microscopy (Fig. 2A2). There appeared to an inhomogeneous distribution of the fluorescent signal due to the presence of non-dye stained w_1 microdroplets inside the dye-carrying hydrophobic phase. Possibly, this was ascribable to the presence of dye-free w_1 droplets. However, due to their minute size, any discontinuity in the red signal associated with w_1 droplets was challenging to discern using conventional microscopy, especially when administering droplets that are only a few microns or less in size. Likely, their non-fluorescent signal was overwhelmed by that emitted by the abundant dye-stained oil phase [44]. This inhomogeneity was obvious for larger w_1 droplets, as displayed by the white arrows in Fig. 2A2. This also indicates that w_1 droplets might promptly coalesce within the continuous oil phase. The instability of the emulsion is directly related to emulsion droplet size and resulting interfacial area, therefore the smaller the droplets the more rapidly they are expected to coalesce, as with many other micro/nano-emulsified systems [45]. Although a sterically stabilising surfactant (i.e. polyoxyethylene sorbitan monolaurate) had been added to w_1, the droplets were thermodynamically prone to separating, due to the large interfacial tension between water and oil phases [46,47]. The coalescence tendency of w_1 droplets within the hydrophobic phase (o) is intimately linked to their physical properties. As mentioned, a relatively high interfacial energy between the dispersed and continuous phases promotes the coalescence of droplets. The coalescence dynamics can also be influenced by the low viscosity of water droplets. This might facilitate the movement of droplets, thereby increasing the incidence of droplet-droplet collisions, while being cognisant of the viscosity of the continuous phase (oil) [48]. Indeed, the emulsion droplets are metastable and move randomly in a continuous phase [49]. Herein, the double emulsion ($w_1/o/w_2$) generated can be successful only if the precursor droplets (w_1) are sufficiently small to remain within the oil phase enabling them to deliver the reacting anion (CO_3^{2-}) effectively for the encapsulation process [50]. Unlike Fig. 2A2, in Fig. 2B2, no w_1 droplets were observed under fluorescence four hours after inducing the interfacial mineralisation. Although the inorganic shell building up around the HS droplets by crystal accretion may have obscured the fluorescent signal, it cannot be excluded that the original droplets may

have coalesced and eventually migrated through the $CaCO_3$ porous crystals into the bulk aqueous phase ($w_1 + w_2 + w_3$). Therefore, w_1 likely merged into $w_2 + w_3$ leaving the lone oil droplet behind to form the core of the capsule (Fig. 2 B1–2). Overall, it seemed that a $CaCO_3$ shell was formed using a nanoparticle-stabilised (Pickering) emulsion as a template. Indeed, interfacially deposited (electrosteric stabilisation at the $o/w_2 + w_3$ interface) $CaCO_3$ NPs (not visible by traditional microscopy) likely acted as nucleation kernels leading to large crystals (visible by traditional microscopy) that ripen into the shell accordingly. Consequently, the interfacial nucleation followed by crystal ripening (mineralisation) also suggested that the in-bulk precipitation of independent crystals may have been diminished/hindered, although still possible, as reported by Wang et al. [51]. In addition, the inoculation of divalent calcium ions was gradual to control the reaction kinetics, thus minimising the precipitation of independent $CaCO_3$ crystals in the bulk, and maximising the throughput of interfacially self-assembled crystals [50]. Based on Fig. 2 B1–2, the ensuing microcapsules exhibited a coarse and porous surface. They seemed to possess a core-shell structure which should be validated by SEM.

Preliminary optical analysis of microcapsules is presented in Fig. 3. Specifically, Fig. 3A provides an overview of air-dried (22 ± 1 °C) microcapsules with a spherical shape from the top view via optical microscopy. Upon air-drying, their surface appeared rippled and rough as also documented by Wang et al. [51] and Long et al. [3] for the fabrication of other $CaCO_3$ based microcapsules. These authors have presented shells made of self-assembled crystals occurring with non-smooth, porous surfaces. Alternatively, the surface coarseness may be attributable to some shrinkage due to moisture loss during air drying, as claimed by Patel et al. [52] for biopolymeric microcapsules with a gelatine–shellac shell. Similar findings had been reported in our previous work on HS-entrapping microcapsules within an all-natural fungal chitosan–gum Arabic shell [14] in which the size difference between the moist and dry microcapsules was found to be statistically significant on average, elucidating that shells might shrink as water is removed. In Fig. 3A, eleven relatively spherical microcapsules are shown. There appeared to be mostly hollow microcapsules (10 out of 11) exhibiting their shell scaffolding only, which appeared transparent under optical microscopy [53]. Possibly, their core might have been lost during air drying. Besides, there appeared to be some excess inorganic material from the bulk remaining around the capsules after complete drying, possibly suggesting that the shell structure did not form cohesively. In contrast, only one dark spot was present, suggesting the presence of an oil-laden (full) microcapsule. Interestingly, the outlines of hollow and full microcapsules appeared morphologically similar to each other, showing a spheroidal-like shape with indentations and structural discontinuities (Fig. 3B). When dealing with inorganic crystals, a porous shell outfit is likely expected which may explain the inability of these microcapsules to survive air-drying, as with other carbonate [3] and phosphate based shells [54]. Fig. 3B was captured to show the structural inhomogeneities of the $CaCO_3$ formed by crystal ripening. After drying, the shell remnants confirmed the spherical morphology of microcapsules following the self-assembly of crystals around the spherical oil droplets. When focusing on the inner side, the curvature line appeared fairly smooth without any significant indentation/clefts. This suggests that the shell may have initiated onto the HS droplets as a template stabilised by $CaCO_3$ NPs [55]. Conversely, the outer curvature line appeared ridged and uneven, leading to inhomogeneous shell thicknesses. This suggests that the crystal accretion around the spherical template was not uniform resulting in patchily formed crystal-based shells. This phenomenon might be attributed to the NPs being adsorbed discontinuously onto the droplet surface, consequently forming nucleation kernels for the crystal accretion inhomogeneously. Indeed, Fig. 3B shows collapsed/incomplete microcapsules with significant shell discontinuity. With that being said, poor barrier properties may be expected from these microcapsules, which shall be discussed extensively later.

3.2. Hybrid microcapsules

$CaCO_3$ shells attained via crystal self-assembly may be discontinuous and porous, which can significantly diminish the barrier properties of the ensuing microcapsules. In literature, multiple examples of PDA-decorated architectures, such as membranes, films, and microcapsule shells have recently arisen [1]. As such, PDA is a mechanically soft material that can offer very limited mechanical/structural strength. Therefore, it has been grown onto sacrificial polymeric templates in

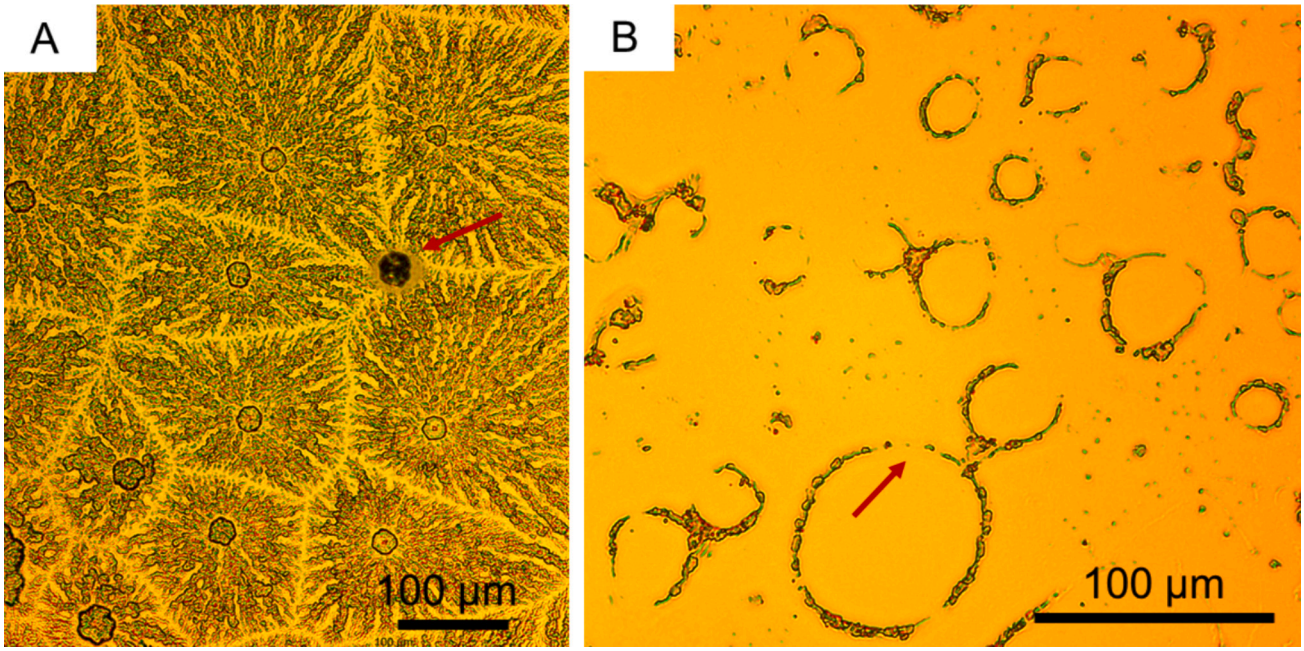

Fig. 3. Top-view optical micrographs of primary microcapsules at different magnifications: (A) oil-laden (dark appearance; see red arrow) versus hollow (transparent) microcapsules with a spherical morphology, air-dried at ambient temperature; (B) partly incomplete (see red arrow) microcapsules with discontinuous/collapsed shells made of $CaCO_3$ crystals, incapable of surviving air drying.

microencapsulation, such as polystyrene, and polyurethane-urea formaldehyde [21], which are microplastic based and hence not environmentally friendly [12]. Dong et al. [56] have proposed the use of composite hollow NPs (~150 nm) made of $CaCO_3$–PDA for potential theragnostic applications. Despite their biocompatibility, their stabilisation required the use of a polyethylene glycol steric film on their surface (PEGylation), which is non-readily degradable, as also listed on the National Library of Medicine in the United States [57,58]. Moreover, no in-depth study entailing inorganic microcapsules (e.g. $CaCO_3$, SiO_2) as stay-in templates for PDA has arisen so far.

The deposition of PDA onto an inorganic substrate (i.e. $CaCO_3$) involves several mechanisms. This process is typically conducted in an alkaline environment (pH 8.5) in the presence of oxygen, enabling dopamine to readily undergo auto-polymerisation. Indeed, oxygen is electrochemically reduced, and its electrons are consumed during the oxidation of dopamine into PDA Ball et al. [32]. The substrate plays a pivotal in the deposition process, providing anchoring sites for the growing PDA layer.

Figure 4 displays the evolution of dopamine from its native monomeric (0 min) into its final polymeric state (24 h) proceeding through multiple reaction intermediates (10–60 min) following the addition of the required buffer solution (sodium tetraborate-HCl_{aq}) at pH 8.5. Noticeably, the gradual change in colouring provides evidence of the forming intermediates (e.g. dopaminochrome) during the pH-driven auto-oxidative process [33]. The chromatic change indicating polymerisation of DPA is concordant with previous literature [59]. Although PDA can be achieved seamlessly within 24 h, the full molecular reaction pathway is unclear due to its complex redox mechanism. However, some authors have attempted to explain the chemical building blocks leading to PDA. At a favourable pH 8.5, Cortés et al. [33] observed the dopamine-inoculated medium to go from colourless (transparent) to deep dark brown as the reaction is completed. This agrees with our findings (Fig. 4) despite the light pinkish chromatic tone at time zero due to the presence of Nile Red. Prior to becoming deep dark brown after 24 h, the reacting medium passed through different shades, namely salmon pink (10 min), persimmon orange (20 min), terracotta clay orange (40 min), and rusty brown (60 min), which possibly corresponded to different reaction intermediates. Based on the Fourier Transform Infrared (FTIR) spectroscopy conducted by Wang et al. [60], the stretching vibrations of the two key carbonyl moieties detected on their first intermediate were likely ascribable to open-chain quinonoid compounds, hence yielding dopamine-quinone. This finding was endorsed by Cortés et al. [33] who have postulated that dopamine-quinone is intermolecularly cyclised to afford leuco-dopaminechrome (10 min) by 1,4-conjugate addition. At this step, the alkaline pH of 8.5 probably acted as the oxidising driving force to enable formation of dopaminechrome together with its tautomer (keto-enol tautomerism), namely indolylquinol (also dihydroxyindole (DHI)) (40–60 min). Further oxidisation over the following 23 h (24 h in total) yielded melanin abundant PDA with a distinctive deep dark brown shade owing to the melanin pigment itself. Cortés et al. [33] tentatively attributed the pH as the key driving force in the self-oxidation process of dopamine, which is also supported by previous contributions in different fields. Richardson et al. have elucidated the leading role of pH as an oxidising agent in the oxidative conversion of phytoplankton-related organo-manganese compounds which could not be activated below pH 8 [61]. An insightful reaction pathway was proposed by Della Vecchia et al. [27] advocating that PDA consists of three key building blocks: acyclised catecholamine-quinones, cyclised DHI segments, and pyrrole-carboxylic acid units. Therefore, the formation of PDA may entail covalently and noncovalently decorated functional moieties, such as indolic/catecholic π-stackings, amino and carbonyl groups. Alternatively, Liu et al. [62] have hypothesised that PDA is mainly built upon noncovalently networked structures of dopamine-quinone and DHI, which are intimately held together by hydrogen, coordination, and electrostatic forces. The broad availability of functional moieties in PDA may justify the excellent mussel-inspired adhesiveness or bonding strength to essentially all types of organic/inorganic substrates including aluminium and polydimethylsiloxane (PDMS) based sheets [63,64].

A protective PDA coating is expected to form around the primary $CaCO_3$ microcapsules, acting as the anchoring sites, after 24 h [21]. Fig. 5 shows the ongoing formation of PDA and/or its precursors after 60 min (Fig. 5A1) and upon completion after 24 h (Fig. 5 B1). The gradual growth of PDA on the primary $CaCO_3$ templates provided the forming microcapsules with a darker rough surface morphology. Moreover, the new hybrid architectures looked relatively compact and self-contained (i.e. structurally intact and not prone to disintegration), likely due to the formation of PDA films that span and stretch onto the porous inorganic surface. Under fluorescence (Fig. 5 A2, 5B2), the PDA-coated microcapsules exhibited enhanced surface roughness confirming the effective self-assembly of the polymer at the surface. Interestingly, the prompt adhesion of PDA onto templates, such as $CaCO_3$, is likely driven by the catechol groups. As reported in the literature, this is possibly due to a combination of covalent, noncovalent, and electrostatic interactions between the catechol functional moieties and various metal ions, including Ca^{2+} [63]. Fig. 5C1 and C2 display the same microcapsule on which PDA is partially formed after ~6 h (incomplete reaction). At different working distances, it was possible to observe a smooth layer of PDA (C1) that had formed onto a highly porous $CaCO_3$ template (C2). However, this was found to be patchy after ~6 h which suggests that the kinetics of formation and subsequent deposition of PDA onto such template was relatively slow, yielding a more homogeneous coating after 24 h (B1, B2).

3.3. Particle size analysis

The size distribution of fresh primary microcapsules (i.e. with only one $CaCO_3$ shell) was determined to be in the range 7 - 75 μm, with a Sauter diameter ($D_{[3,\ 2]}$) of 29.8 ± 2.7 μm (Fig. 6). When aged under stirring for >24 h, such microcapsules did not appear to be solid enough to withstand the shear generated in the vessel. This finding suggests that the inorganic scaffolding provided by the crystals alone may not form cohesively leading to collapsing microcapsules. Unsurprisingly, this seemed to confirm the findings from optical micrographs in which

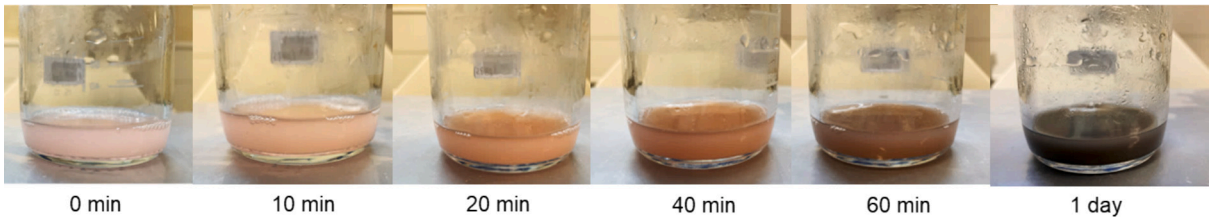

Fig. 4. Photographs of the dopamine loaded formulations collected at specific time intervals (0, 10, 20, 40, 60 min, and 24 h) showing a heavy chromatic change. The reacting medium exhibited different chromatic shades at different times: pinkish transparent (0 min) salmon pink (10 min), persimmon orange (20 min), terracotta clay orange (40 min), and rusty brown (60 min), and deep dark brown (after 24 h).The formulations were prepared with dopamine hydrochloride (3.5 g/L) within a sodium tetraborate-HCl_{aq} solution) at pH 8.5.

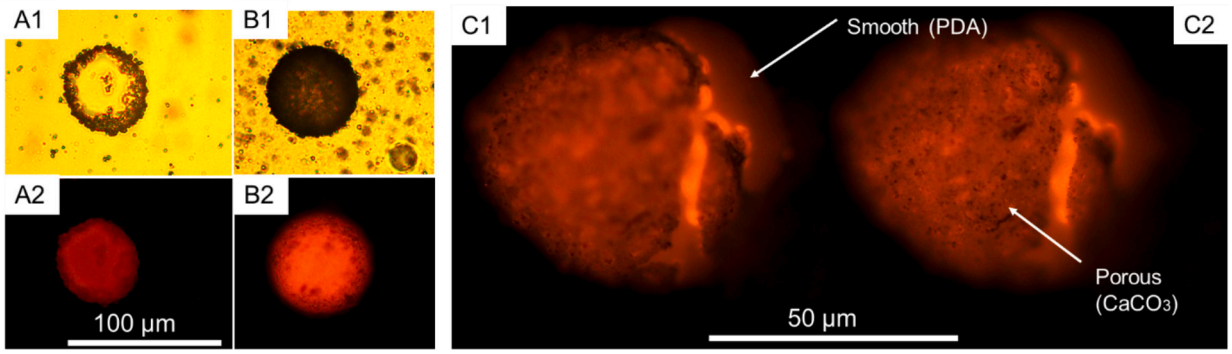

Fig. 5. Top-view optical micrographs of (A) PDA forming around $CaCO_3$ shells after 60 min (incomplete reaction) and (B) PDA-coated microcapsules after 24 h (complete reaction); C1-C2 displays the hybrid inorganic-organic ($CaCO_3$-PDA) structure of the resulting microcapsules after 60 min (incomplete deposition of PDA). Both C1 and C2 were captured from the same microcapsule at two different working distances, allowing the observation of the microcapsule (3D structure) at slightly different observation planes. This facilitated a high resolution and sharp focus of the details of interest, namely the outer PDA coating (C1; see arrow) and the $CaCO_3$ microporous structure beneath (C2; see arrow).

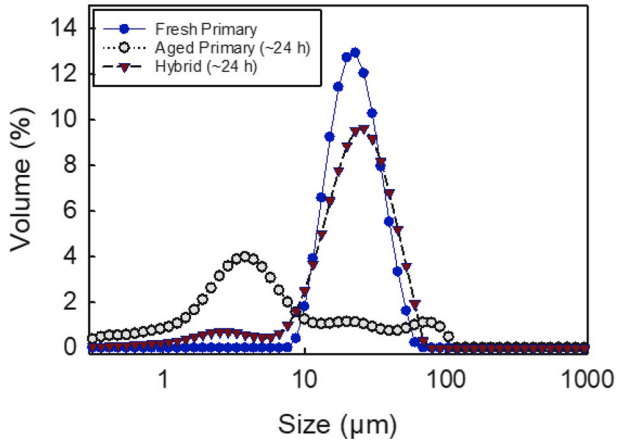

Fig. 6. Size distribution of fresh (●) and aged (~24 h; ○) primary and hybrid (▼) microcapsules.

collapsed microcapsules together with their inorganic residues were found (Fig. 3B). Likely, these microcapsules lost their oil load whilst being stirred leading to shrinkage and hence a significantly lower mean Sauter diameter of 6.4 ± 0.1 µm. In addition, the size distribution curve of aged primary microcapsules was significantly wider. Moreover, their peak intensity (~4%) was much lower than that of the fresh primary ones (~13%). Unlike other literature reports, we present the size distribution of fresh hybrid microcapsules as well. The mean Sauter diameter of PDA-coated hybrid microcapsules was 31.2 ± 0.4 µm showing no statistically significant difference with that observed from primary microcapsules. This result was not surprising since PDA is expected to form very thin coatings in the range of 50–100 nm, as reported by Li et al. [28]. Indeed, the measurement yielded a single-peak size distribution developing within the subtended bell-shaped area of the curve of primary microcapsules (Fig. 6). This suggests that the hybrid microcapsules formed onto the $CaCO_3$ templates effectively. However, the peak value of the hybrid microcapsules was around 3% weaker than that of the primary ones. This might be related to the slight hint of peak in the 1-10 µm region, suggesting that a population of primary microcapsules might have shrunk prior to getting coated by PDA within the 24 h secondary encapsulation window, due to oil core loss or shear-triggered crystal disassembling. We have hypothesised that PDA may form onto the inorganic ($CaCO_3$) templates by coating and linking the shell crystals, which had previously self-assembled around the oil core. Thus, PDA may provide a plasticised-like soft protective film capable of keeping the inorganic structure in place. However, such postulation should be validated following an in-depth mechanical analysis of both primary and hybrid microcapsules, which has not been reported thus far.

3.4. Scanning electron microscopy

SEM images of primary (A,B,C) and hybrid microcapsules (D,E,F) are presented in Fig. 7. Primary $CaCO_3$ microcapsules were found to be spherically shaped (A, B). They appeared to be reasonably well dispersed although aggregated particles were present as well. Incomplete and through-hole like microcapsules were also visible (C) suggesting that the core may have leaked out, leading to hollow $CaCO_3$ microparticles and mineral scraps. Similar results were also presented by Yuan et al. [65], who reported $CaCO_3$ microparticles with topographic properties similar to those presented in this work (relative surface smoothness), associated with the presence of micro-scale $CaCO_3$ (vaterite) following FTIR assay. It is well understood that carbonates may occur with multiple crystal polymorphs [66]. We also found smooth surfaces. However, as with many other near-zero conductive ceramic materials ($CaCO_3$ conductivity $4.5{\cdot}10^{-6}$ S·cm^{-1} at 16 °C [67]), high resolution imaging may be impaired resulting in blurry images. With that being said, mesoporosity and surface coarseness may still not be visible although a thin (~8 nm) conductive platinum ($9.43{\cdot}10^{6}$ S·cm^{-1}) layer had been purposely deposited [68]. EDX analysis confirmed the presence of $CaCO_3$ (Supplementary Material S1). Furthermore, the inset (Fig. 7A1) shows several dry residues of $CaCO_3$ crystals that appear significantly less rough than those presented by Wang et al. [51]. The curved residue was likely part of a former microcapsule shell that had broken apart, possibly suggesting intrastructural weakness among the crystals. A systematic mechanical analysis is presented later. When comparing $D_{[2,3]}$ = 29.8 ± 2.7 µm (under moist conditions by laser diffraction) with the averaged diameter of 4.4 ± 1.4 µm (under dry conditions from SEM micrograph 6 A-C analysed using ImageJ), a substantial difference arose. This seemed to confirm that the shrinkage of $CaCO_3$ microcapsules was not negligible due to drying and liquid core loss [12].

Figure 7D displays an overview of three hybrid microcapsules with a spherical morphology. As can be seen, the outer surface appeared relatively rough owing to the top-deposited PDA coating. They seemed to have similar sizes in the range of 25–30 µm, which was consistent with the size provided by laser diffraction ($D_{[2,3]}$ =31.2 ± 0.4 µm). Unlike primary microcapsules, this suggested PDA provided a protective layer capable of enhancing the structural integrity of microcapsules, thereby preventing $CaCO_3$ crystals from self-dismantling (A1). Possibly, PDA coated microcapsules possessed a mesoporous structure beneath which a dense microporous mantle of $CaCO_3$ crystals occurred (Fig. 7E, see red

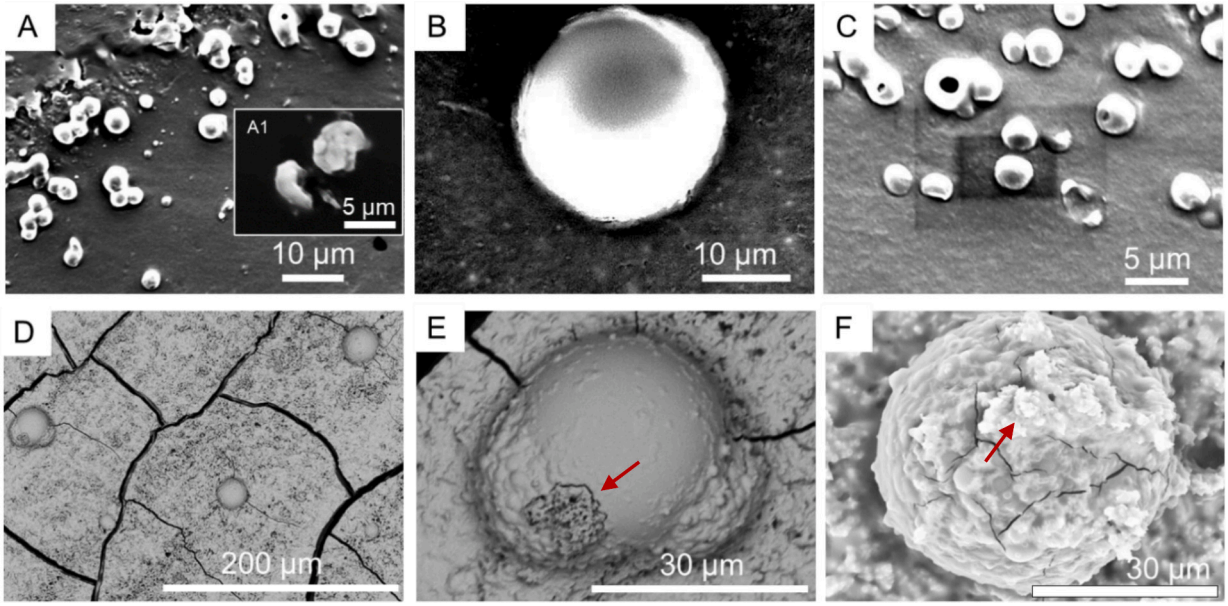

Fig. 7. SEM micrographs of primary (A, B, C) and hybrid (D, E, F) microcapsules.

arrow). Another typical example of a PDA-coated microcapsule with a sprout-like appearance is presented in Fig. 7F. Its surface was coarse with dimples, creases, and crusts/lumps which might be ascribable to some surplus PDA having adhered irregularly during the 24 h secondary encapsulation window. Alternatively, these uneven lumps, highlighted by the red arrow, might be due to excess $CaCO_3$ NPs aggregating at the outer surface of microcapsule [28]. Moreover, a few randomly oriented fractures were visible at the microcapsule surface. This is likely due to the presence of the soft, thin (<100 nm [21]) outermost PDA layer, which may be sensitive to vacuum conditions and the electron beam during prolonged SEM imaging at high accelerating voltage.

3.5. Mechanical properties

The rupture force of hybrid microcapsules in a dry form as a function of their diameter is presented in Fig. 8A. As can be seen, there appeared a clear increase of the rupture force with diameter. This finding was also concordant with the trend of many other types of microcapsules with similar or different shell chemistries (e.g. chitosan-gum Arabic [16], melamine-formaldehyde [35], and calcium carbonate-melamine formaldehyde (CCMF) [69]). The nominal rupture stress (rupture force/cross sectional area of the particle) was found to decrease with the diameter (Fig. 8B), as also seen in several former reports [12]. Interestingly, the average nominal rupture stress of hybrid microcapsules (2.2 ± 0.3 MPa) was around four-fold as high as that of other lab-made CCMF microcapsules with similar size, as reported in literature (0.54 ± 0.06 MPa) [3]. Most importantly, they exhibited values of rupture stress comparable to those of commercial MF (1.2–1.8 MPa) and melamine based-polyurea (PU) microcapsules (1.5 MPa) with similar sizes (~31 μm) for detergent applications [70]. PDA-coated hybrid microcapsules with mean number-based diameter 30.0 ± 2.0 μm yielded relatively high nominal rupture stress values, which can be appealing to a broad variety of industrial sectors [34]. The number-based diameter of the hybrid microcapsules from micromanipulation measurements was in excellent agreement with that detected via laser diffraction (31.2 ± 0.4 μm), suggesting that microcapsule shrinking due to drying may be negligible/limited in contrast to other fully organic microcapsules (e.g. chitosan-gum Arabic) [12]. Fig. 8C displays the displacement at rupture of hybrid microcapsules, which seems to increase with their diameter. Their nominal deformation at rupture (derived from the slope of the displacement at rupture vs diameter curve) was relatively low (9.9 ± 1.6%) suggesting that the hybrid microcapsules might get shattered early under compression, which is concordant with other $CaCO_3$ NP-stabilised microcapsules (7.5 ± 0.4%) presented by Long et al. [71]. For completion, the diameter-independent rupture tension (rupture force/initial diameter of the particle) was determined to be 44.0 ± 6.1 $N{\cdot}m^{-1}$. Interestingly, this value appeared similar to that reported in literature for polymeric MF microcapsules (35–47 $N{\cdot}m^{-1}$) [70,72]. It is noteworthy to say that $CaCO_3$ crystal as such were incapable of withstanding drying and/or shear, and collapsed (Fig. 3B,6). PDA may have acted as a fixating agent to 'glue' the inorganic crystals together around the oil cores resulting in well-formed shells (Fig. 7D—F). Indeed, it is worth mentioning that the hybrid microcapsules were fabricated inexpensively, without any high energy consumption methodology or costly platinum/gold NPs templates to sustain metallic microcapsule shells, as previously reported [73,74]. The key mechanical parameters of PDA-coated $CaCO_3$ microcapsules in comparison with other microcapsule chemistries are listed below (Table 1). The PDA-$CaCO_3$ microcapsules prepared under the conditions investigated were significantly stronger than MF-$CaCO_3$ microcapsules, but marginally weaker than PU-MF or fungal chitosan (fCh)-gum Arabic (GA) microcapsules based on the values of their nominal rupture stress. It should be pointed out that the mechanical strength of microcapsules for a given application should be in an optimal range [70], if the release of the encapsulated active ingredient needs to be triggered using mechanical forces. The PDA-$CaCO_3$ microcapsules as shown in Table 1 had sufficient mechanical strength, at least for detergent applications [70]. Micromanipulation compression tests of hybrid microcapsules have been filmed and made available as Supplementary Material (S2).

3.6. Retention of active oil

The barrier properties of PDA-coated and non-PDA coated calcium carbonate shells were assayed by triggering the release of HS into a fresh water environment at pH 9 as the receptor medium (solubility of HS in water at ambient temperature ~ 10 mg/L [15]) under magnetic stirring. Firstly, both payload (30.6 ± 0.1%) and encapsulation efficiency (44.2 ± 0.2%) of microcapsules were calculated to assure the total HS load within the microcapsules (0.6 mg) to be well below its solubility limit during the release experiments. No significant difference in the payload between primary and hybrid microcapsule was found since only 42.5 mg

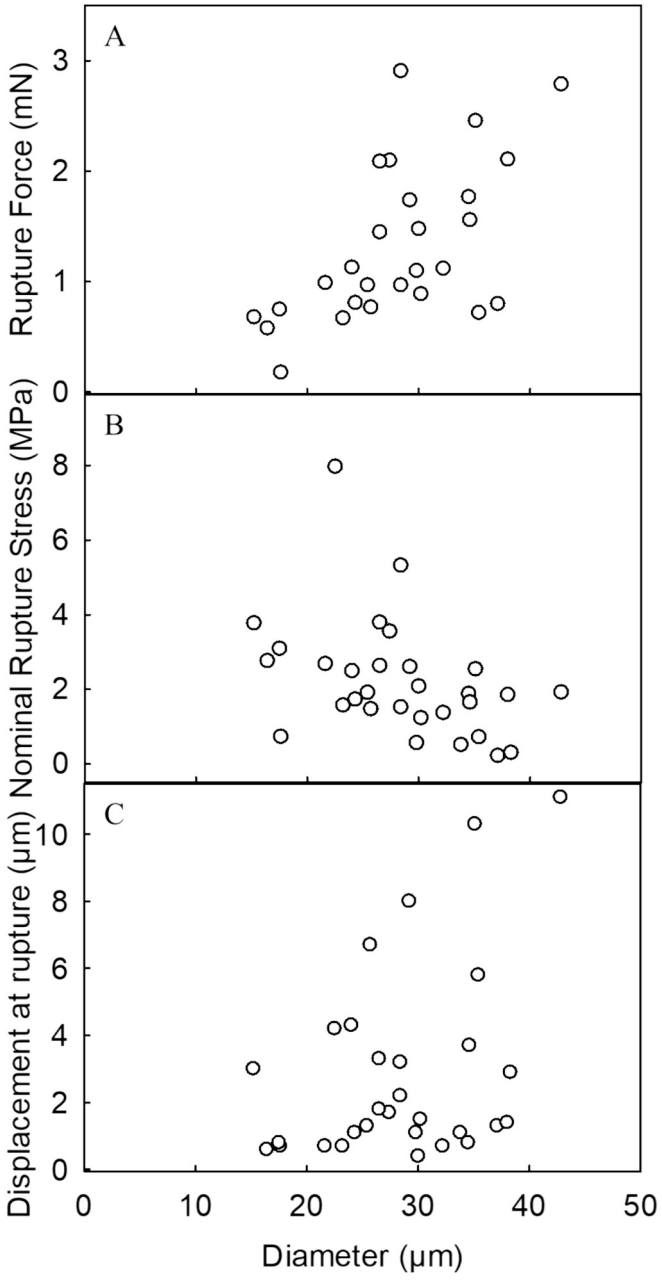

Fig. 8. Key mechanical property parameters of hybrid (O) microcapsules versus their diameter: rupture force (A), nominal rupture stress (B), displacement at rupture (C).

of monomeric dopamine was employed for the secondary encapsulation. The mass of HS cumulatively released into the receptor medium was measured up to 30 days (Fig. 9) by UV–Vis spectroscopy. As shown in the inset to Fig. 9, the primary microcapsules were observed to release the whole oil load within ~4 h, whereas no release signal was detectable from the hybrid microcapsules after 24 h. In contrast, the $CaCO_3$-only microcapsules, produced by Long et al. [3], released ~2.3% after 24 h. Evidently, the rapid loss from primary microcapsules indicated mostly defective/incomplete shells, which triggered a fast release of the core into the receptor medium (bulk). In contrast, the release rate of hybrid microcapsules was determined to be much slower. Indeed, the release profile of hybrid microcapsules was non-linear over 30 days at which point around 40% of the total oil was released. From the inset of Fig. 9, there appeared to be an initial 'lag time', where no release signal from the oil was detected within the first 4 h. This suggests that the diffusional

Table 1
Key mechanical property parameters of PDA-coated $CaCO_3$ microcapsules (mean ± standard error) in comparison with other microcapsule types: (i) MF-$CaCO_3$ [3], (ii) polyurea (PU)–MF [75], and (iii) glutaraldehyde-crosslinked fungal chitosan (fCh)–gum Arabic (GA) microcapsules [16].

	PDA-$CaCO_3$	MF-$CaCO_3$	PU-MF	fCh-GA
Number-based diameter (µm)	30.0 ± 2.0	15.4 ± 1.3	25.1 ± 6.8	27.5 ± 1.5
Rupture Force (mN)	1.32 ± 0.15	0.09 ± 0.01	1.8 ± 0.8	2.0 ± 0.1
Rupture Tension ($N \cdot m^{-1}$)	44.0 ± 6.1	–	69.6 ± 14.7	72.2 ± 6.5
Nominal Rupture Stress (MPa)	2.2 ± 0.3	0.54 ± 0.06	3.7 ± 0.7	3.6 ± 0.3
Displacement at Rupture (µm)	2.9 ± 0.5	1.1 ± 0.1	8.9 ± 3.6	6.3 ± 3.1
Deformation at Rupture (%)	9.9 ± 1.6	7.3 ± 0.5	35.8 ± 11.6	22.7 ± 1.5
Reference	–	Long et al. [3]	Hu et al. [75]	Baiocco et al. [16]

mass transfer mechanism of the oil through the inorganic-organic dual shell was negligible or well below the sensitivity threshold of the instrument (i.e. nil signal). Subsequently, a jump release to ~10% was observed from PDA-coated microcapsules after around 24 h (Fig. 9) followed by a further relatively rapid release to ~20% after approximately 48 h. Thereafter, the oil continued to be released (i.e. gradual rise to a maximum), which seemed to gradually slow down over the following ~4 weeks. Overall, both primary and hybrid microcapsules exhibited nonlinear release profiles over significantly different time periods, which should be directly reflected in their characteristic diffusion times (φ) [s]. As presented in our previous works, the release function can be described by the following nonlinear regression [4,34]:

$$R(t) = \xi\left(1 - e^{t/\varphi}\right) \quad (1)$$

where $R(t)$ is the dimensionless cumulative released oil (operative range 0–1 or 0–100%) at time t [s] and ξ is the dimensionless pre-exponential factor associated with an individual microcapsule, which can be considered constant.

The characteristic diffusion times were determined to be (3.57 ± 0.35) × 10^3 s and (1.26 ± 0.14) × 10^6 s for the primary and hybrid microcapsules, respectively. Interestingly, the characteristic diffusion time associated with the PDA-coated microcapsules was approximately three orders of magnitude greater than that of the primary ones. This possibly suggested a significantly slower diffusion rate of the oil (HS) through the shell of hybrid microcapsules. Indeed, the influence of PDA as the outermost coating seemed to have played a key role in mitigating the overall oil leakage, in comparison with the primary $CaCO_3$ microcapsules which did not appear suitable for retaining the oil due to its inner porosity and the noncontinuous assembly of the crystals. This finding is also reflected in the corresponding ξ values that represent the asymptotic/limiting behaviour of the diffusional process of the oil through the shell. Specifically, primary and hybrid microcapsules yielded ξ values of 93.1 ± 3.6% and 48.6 ± 3.3%, respectively. Based on the data, the primary microcapsules reached values close to 100%, evidencing that nearly the whole active load facilely diffused through their shell, which is made of $CaCO_3$ alone, and hence suggesting poor barrier properties. In contrast, the ξ value of hybrid microcapsules was roughly half that of the primary ones, elucidating the reduced capability of the oil to be transferred into the receptor medium through the hybrid inorganic-organic shell, and hence enhanced barrier properties. Alternatively, it cannot be excluded that the perfume oil might exhibit some natural affinity for the organic network. Consequently, the oil may possibly get trapped within the organic shell via partial solubilisation, as also presented in our previous work for biopolymer based coacervate

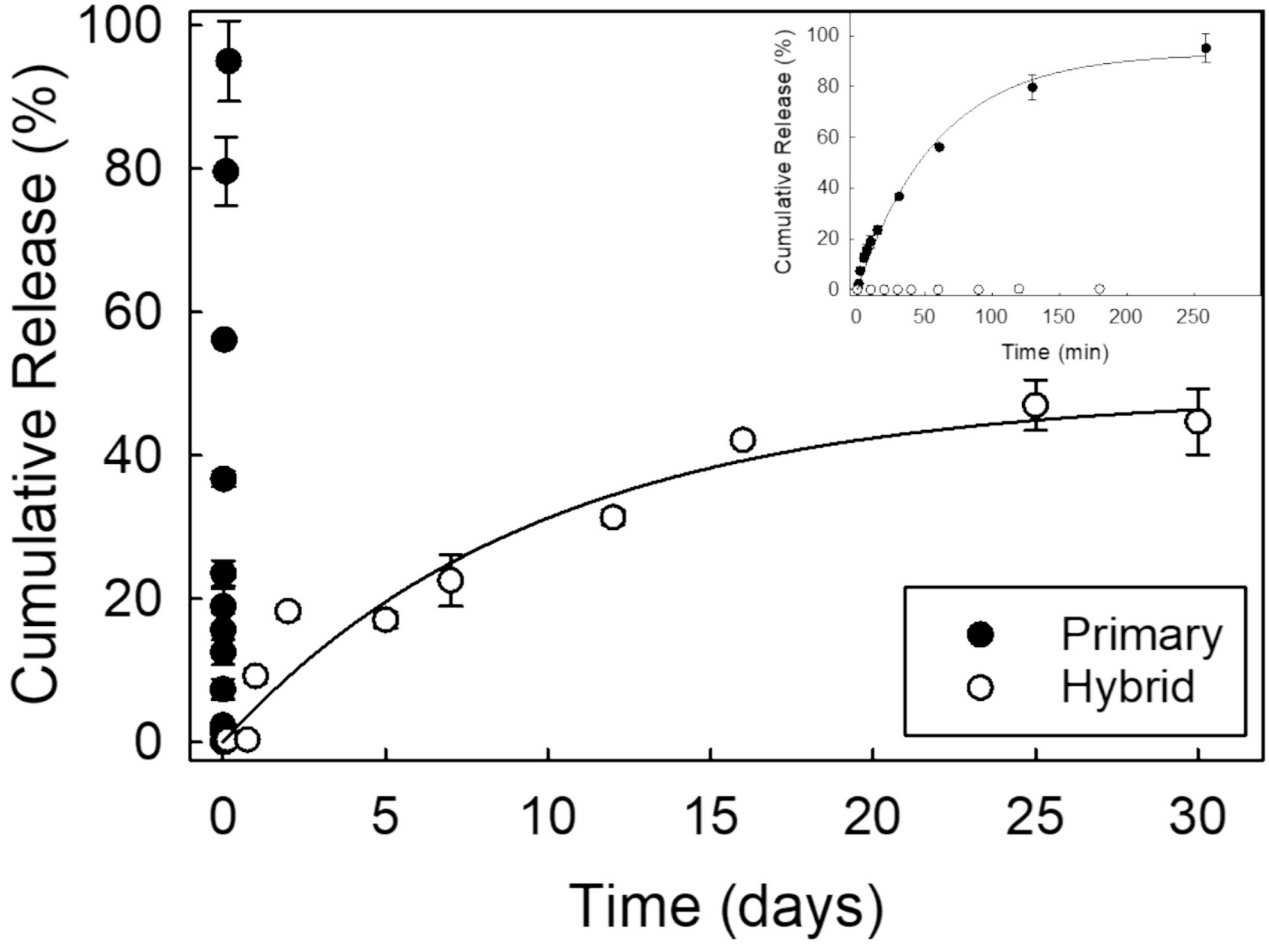

Fig. 9. Time-dependent cumulative release of HS from primary (●) and hybrid (O) microcapsules in absolute water. The inset displays the release of HS from both types of microcapsules within ~4 h. Some error bars are not visible because they are smaller than the size of symbols. The solid curves represent the curve-fit nonlinear regressions of the cumulative release (Eq.1) generated via Sigma Plot 14.5 ($p < 0.0001$; Alfasoft, Gothenburg, Sweden, EU), as also presented in our previous work [4].

shells [14]. Overall, the results suggest that PDA coatings might form continuously around the $CaCO_3$ templates, offering a substantial mass transfer resistance to prevent undesirable burst releases. However, these capsules are still not currently capable of achieving zero leakage for which research is still ongoing.

3.7. Microcapsule adhesiveness

The adhesive properties of microcapsules were tested using a microfluidic device fitted with a smooth crimp-free PET substrate. The results enabled us to understand the effect of PDA on the adhesive properties of microcapsules [12]. Fig. 10 displays the retention performance of both primary and hybrid microcapsules onto a PET substrate as a function of the applied hydrodynamic shear stress (τ) and the corresponding Reynolds number (*Re*) in moist conditions. Fully detailed mathematical equations can be found in our previous work [12]. As reported in literature, industrial microcapsules are often exposed to both laminar and turbulent regimes in their end-use applications [12]. Specifically, when dealing with laundry applications, the microcapsules are likely subjected to a turbulent regime during the washing/drying cycles, whereas their flow through the rectangular/round microchannels of the fabrics is possibly laminar [16,76]. At a detergent-like pH of 9, the retention performance of the primary microcapsules was found to drop dramatically from 100% to ~25% at Re ~ 1–2. This suggests that most of these capsules were not capable of adhering firmly onto the PET substrate, and hence were flushed away. By contrast, no significant drop

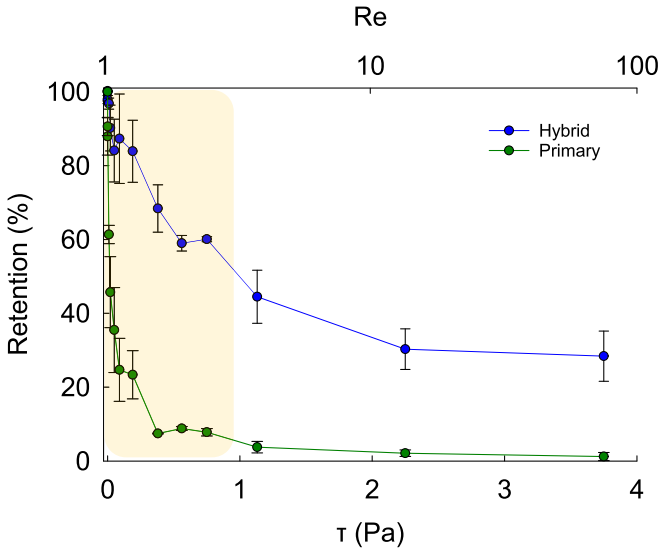

Fig. 10. Retention performance of primary and hybrid microcapsules onto thin PET substrates (thickness ~ 0.25 ± 0.02 mm) as a function of hydrodynamic shear stress (τ) and Reynolds number (*Re*; secondary *x*-axis) at a detergent pH of 9.

was observed from hybrid microcapsules under the same conditions. At Re ~ 1–2 the retention performance of hybrid microcapsules was higher than 85%. As the hydrodynamic shear stress was increased to $\tau \geq 0.45$ Pa (Re $\simeq$ 3), the retention performance of hybrid microcapsules gradually decreased to ~65%, whereas that of primary capsules was <10%. As reported by Liu [76], $\tau \simeq 0.9$ Pa corresponds to the threshold hydrodynamic shear stress (Re $\simeq$ 4.5) that perfume microcapsules should be withstanding, at least, during washing/drying cycles. A significant difference between primary and hybrid microcapsules was observed at this shear stress value. Specifically, the retention performance of hybrid microcapsules was determined to be ~60% while that of primary microcapsules was below 10%. Above this threshold value, the trend of both capsule samples appeared similar and decreased significantly as the shear is pushed above $Re > 10$ corresponding to moderately high flowrates (>20 mL/min). Above Re ~10, the curve seemed to decrease marginally. Additionally, at $Re \simeq 90$, PDA-coated microcapsules were still found to adhere significantly better than the primary ones (>5%) yielding a higher retention performance (~35%). PDA-coated microcapsules were found to be ~35–40% more adhesive onto PET substrates when compared to commercial synthetic (MF-based) microcapsules (corresponding retention performance ~25%) tested by a similar microfluidic device operating at a hydrodynamic shear stress (HSS) of ~0.5 Pa, as reported by Liu [76]. Similarly, He et al. [77] assayed perfume-laden MF (supplied by Procter & Gamble, Brussels Innovation Centre, Brussels, Belgium) for their adhesion onto a cellulose film. As such, MF microcapsules were able to cover only ~10% of the exposed cellulose surface at a HSS of ~0.04 Pa, likely confirming the poor adhesive properties of synthetic resins to model substrate without any surface modification. Overall, it can be inferred that PDA coatings enhanced microcapsule-PET substrate adhesion effectively, with a potential for multiple industrial applications.

4. Conclusions

A facile, inexpensive, and eco-friendly methodology relying on the template-mediated oxidative auto-polymerisation of dopamine to form PDA onto $CaCO_3$ shells was investigated to fabricate robust hybrid organic-inorganic microcapsules with a core of model perfume oil (HS). Individual and spherically shaped hybrid microcapsules were obtained. The dense $CaCO_3$ shell was highly porous, whereas the outermost PDA coating was found to be more homogeneous and intact. The fluorescence sensing properties of the active core (i.e. Nile red dyed HS) provided evidence that the oil was retained successfully during primary and secondary encapsulation. In a typical liquid detergent pH 9, ~40% of HS was released from the hybrid microcapsules after one month, whereas a sudden release (within 4 h) was observed from the primary ones. In dry conditions, the PDA-coated microcapsules were determined to be mechanically strong, with a rupture tension of 44.0 ± 6.1 N·m^{-1}, which is similar to that associated with other synthetic lab-made [78] and commercial MF microcapsules [70]. Furthermore, the adhesion of primary and hybrid microcapsules onto model PET substrates were assessed when exposed to a simulated liquid detergent with a pH of 9. Under low ($Re \simeq$ 1–2), moderate ($Re \simeq 4.5$), and relatively high ($Re \simeq 90$) hydrodynamic shear stress, it was found that PDA-coated microcapsules exhibited an absolute retention of ~85%, ~60%, and ~ 35% on PET films, whereas that of primary ones was about 25%, 10%, and 5%. Indeed, PDA-coated microcapsules also demonstrated enhanced adhesion onto PET substrates, when compared to commercial MF microcapsules without any surface modification (retention performance ~25% at moderate Re). Promisingly, this rationally integrated hybrid architecture may provide safe and relatively stable microcapsules to be fabricated inexpensively without any high energy consumption. The fabrication consists of two key processes: emulsification followed by encapsulation, which all were conducted in a stirred vessel with temperature control. Such processing equipment are widely used in industry, and it is possible to reliably scale up the fabrication processes. Nevertheless, a comprehensive technoeconomic analysis of the whole manufacturing process should be conducted in collaboration with industry and allied regulatory bodies before such microcapsules can be produced at a large scale. Overall, such microcapsules may be appealing for a broad range of potential applications where sustained release of the active is required, as well as environmentally benign and user-friendly microcapsules with readily tuneable mechanical, barrier and surface properties are desirable.

Supplementary data to this article can be found online at https://doi.org/10.1016/j.susmat.2024.e01001.

CRediT authorship contribution statement

Daniele Baiocco: Writing – review & editing, Writing – original draft, Visualization, Validation, Supervision, Software, Resources, Methodology, Investigation, Formal analysis, Data curation, Conceptualization. **Benjamin T. Lobel:** Writing – review & editing, Investigation. **Mohammed Al-Sharabi:** Writing – review & editing, Formal analysis. **Olivier J. Cayre:** Writing – review & editing, Funding acquisition. **Alexander F. Routh:** Writing – review & editing, Supervision, Funding acquisition. **Zhibing Zhang:** Writing – review & editing, Supervision, Resources, Project administration, Funding acquisition, Data curation, Conceptualization.

Declaration of competing interest

The authors declare no conflict of interest regarding the research, authorship, and publication of this article.

Data availability

Data will be made available on request.

Acknowledgments

This work was supported by EPSRC, UK [Grant Numbers EP/V027654/1, EP/V027727/1, EP/V027646/1].

References

[1] Z. Wang, C. Li, J. Xu, K. Wang, X. Lu, H. Zhang, S. Qu, G. Zhen, F. Ren, Bioadhesive microporous architectures by self-assembling polydopamine microcapsules for biomedical applications, Chem. Mater. 27 (3) (2015) 848–856.
[2] Y. Zhang, D. Baiocco, A.N. Mustapha, X. Zhang, Q. Yu, G. Wellio, Z. Zhang, Y. Li, Hydrocolloids: nova materials assisting encapsulation of volatile phase change materials for cryogenic energy transport and storage, Chem. Eng. J. 382 (2020) 123028.
[3] Y. Long, B. Vincent, D. York, Z. Zhang, J.A. Preece, Organic-inorganic double shell composite microcapsules, Chem. Commun. (Camb.) 46 (10) (2010) 1718–1720.
[4] D. Baiocco, J.A. Preece, Z. Zhang, Microcapsules with a fungal chitosan-gum arabic-maltodextrin shell to encapsulate health-beneficial peppermint oil, Food Hydrocoll. Health 1 (2021) 100016.
[5] Y. Zhang, A.N. Mustapha, X. Zhang, D. Baiocco, G. Wellio, T. Davies, Z. Zhang, Y. Li, Improved volatile cargo retention and mechanical properties of capsules via sediment-free in situ polymerization with cross-linked poly(vinyl alcohol) as an emulsifier, J. Colloid Interface Sci. 568 (2020) 155–164.
[6] J. Li, M.A.J. Mazumder, H.D.H. Stöver, A.P. Hitchcock, I.M. Shirley, Polyurea microcapsules: surface modification and capsule size control, J. Polym. Sci. A Polym. Chem. 49 (14) (2011) 3038–3047.
[7] H. Li, R. Wang, H. Hu, W. Liu, Surface modification of self-healing poly(urea-formaldehyde) microcapsules using silane-coupling agent, Appl. Surf. Sci. 255 (5, Part 1) (2008) 1894–1900.
[8] E. Katoueizadeh, S.M. Zebarjad, K. Janghorban, Morphological study of surface-modified urea–formaldehyde microcapsules using 3-aminopropyltriethoxy silane, Polym. Bull. 76 (3) (2019) 1317–1331.
[9] A.H. Navarchian, N. Najafipoor, F. Ahangaran, Surface-modified poly(methyl methacrylate) microcapsules containing linseed oil for application in self-healing epoxy-based coatings, Prog. Org. Coat. 132 (2019) 288–297.
[10] P.J. Ong, Z.M. Png, X.Y. Debbie Soo, X. Wang, A. Suwardi, M.H. Chua, J.W. Xu, Q. Zhu, Surface modification of microencapsulated phase change materials with nanostructures for enhancement of their thermal conductivity, Mater. Chem. Phys. 277 (2022) 125438.
[11] L. Hu, X. Li, L. Ding, L. Chen, X. Zhu, Z. Mao, X. Feng, X. Sui, B. Wang, Flexible textiles with polypyrrole deposited phase change microcapsules for efficient

photothermal energy conversion and storage, Sol. Energy Mater. Sol. Cells 224 (2021) 110985.
[12] D. Baiocco, Z. Zhang, Microplastic-free microcapsules to encapsulate health-promoting limonene oil, Molecules 27 (2022).
[13] S. Lu, J. Xing, Z. Zhang, G. Jia, Preparation and characterization of polyurea/polyurethane double-shell microcapsules containing butyl stearate through interfacial polymerization, J. Appl. Polym. Sci. 121 (6) (2011) 3377–3383.
[14] D. Baiocco, Z. Zhang, Y. He, Z. Zhang, Relationship between the Young's moduli of whole microcapsules and their shell material established by micromanipulation measurements based on diametric compression between two parallel surfaces and numerical modelling, Micromachines 14, (1) (2023) 123.
[15] D. Baiocco, Fabrication and Characterisation of Vegetable Chitosan Derived Microcapsules, PhD Thesis, University of Birmingham, 2021.
[16] D. Baiocco, J.A. Preece, Z. Zhang, Encapsulation of hexylsalicylate in an animal-free chitosan-gum Arabic shell by complex coacervation, Colloids Surf. A Physicochem. Eng. Asp. 625 (2021) 126861.
[17] F. Yu, C. Xue, Z. Zhang, Mechanical characterization of fish oil microcapsules by a micromanipulation technique, LWT 144 (2021) 111194.
[18] J. Yeom, W.S. Shim, N.G. Kang, Eco-friendly silica microcapsules with improved fragrance retention, Appl. Sci. 12 (2022) 6759.
[19] H. Bahrom, A.A. Goncharenko, L.I. Fatkhutdinova, O.O. Peltek, A.R. Muslimov, O. Y. Koval, I.E. Eliseev, A. Manchev, D. Gorin, I.I. Shishkin, R.E. Noskov, A.S. Timin, P. Ginzburg, M.V. Zyuzin, Controllable synthesis of calcium carbonate with different geometry: comprehensive analysis of particle formation, cellular uptake, and biocompatibility, ACS Sustain. Chem. Eng. 7 (23) (2019) 19142–19156.
[20] F. Ponzio, J. Barthès, J. Bour, M. Michel, P. Bertani, J. Hemmerlé, M. d'Ischia, V. Ball, Oxidant control of Polydopamine surface chemistry in acids: a mechanism-based entry to superhydrophilic-superoleophobic coatings, Chem. Mater. 28 (13) (2016) 4697–4705.
[21] S. Kang, M. Baginska, S.R. White, N.R. Sottos, Core–Shell polymeric microcapsules with superior thermal and solvent stability, ACS Appl. Mater. Interfaces 7 (20) (2015) 10952–10956.
[22] B. Poinard, S.A.E. Lam, K.G. Neoh, J.C.Y. Kah, Mucopenetration and biocompatibility of polydopamine surfaces for delivery in an ex vivo porcine bladder, J. Control. Release 300 (2019) 161–173.
[23] X. Liu, J. Cao, H. Li, J. Li, Q. Jin, K. Ren, J. Ji, Mussel-inspired polydopamine: a biocompatible and ultrastable coating for nanoparticles in vivo, ACS Nano 7 (10) (2013) 9384–9395.
[24] C. Tang, Y. Li, J. Pun, A.S. Mohamed Osman, K.C. Tam, Polydopamine microcapsules from cellulose nanocrystal stabilized pickering emulsions for essential oil and pesticide encapsulation, Colloids Surf. A Physicochem. Eng. Asp. 570 (2019) 403–413.
[25] A. Zou, Y. Yang, J. Cheng, V.M. Garamus, N. Li, Construction and characterization of a novel sustained-release delivery system for hydrophobic pesticides using biodegradable polydopamine-based microcapsules, J. Agric. Food Chem. 66 (25) (2018) 6262–6268.
[26] J. Wang, Y. Lv, An enzyme-loaded reactor using metal-organic framework-templated polydopamine microcapsule, Chin. J. Chem. Eng. 29 (2021) 317–325.
[27] N.F. Della Vecchia, R. Avolio, M. Alfè, M.E. Errico, A. Napolitano, M. d'Ischia, Building-block diversity in Polydopamine underpins a multifunctional eumelanin-type platform tunable through a Quinone control point, Adv. Funct. Mater. 23 (10) (2013) 1331–1340.
[28] H. Li, Y. Jia, X. Feng, J. Li, Facile fabrication of robust Polydopamine microcapsules for insulin delivery, J. Colloid Interface Sci. 487 (2017) 12–19.
[29] T. Sun, Z.-J. Li, H.-G. Wang, D. Bao, F.-L. Meng, X.-B. Zhang, A biodegradable Polydopamine-derived electrode material for high-capacity and Long-life Lithium-ion and sodium-ion batteries, Angew. Chem. Int. Ed. 55 (36) (2016) 10662–10666.
[30] K.J. Mehta, Iron oxide nanoparticles in mesenchymal stem cell detection and therapy, Stem Cell Rev. Rep. 18 (7) (2022) 2234–2261.
[31] R.A. Robinson, J.B. Macaskill, Osmotic coefficients of aqueous sodium carbonate solutions at 25°C, J. Solut. Chem. 8 (1) (1979) 35–40.
[32] V. Ball, D.D. Frari, V. Toniazzo, D. Ruch, Kinetics of Polydopamine film deposition as a function of Ph and dopamine concentration: insights in the Polydopamine deposition mechanism, J. Colloid Interface Sci. 386 (1) (2012) 366–372.
[33] M.T. Cortés, C. Vargas, D.A. Blanco, I.D. Quinchanegua, C. Cortés, A.M. Jaramillo, Bioinspired polydopamine synthesis and its electrochemical characterization, J. Chem. Educ. 96 (6) (2019) 1250–1255.
[34] R. Mercade-Prieto, R. Allen, D. York, J.A. Preece, T.E. Goodwin, Z. Zhang, Determination of the shell permeability of microcapsules with a core of oil-based active ingredient, J. Microencapsul. 29 (5) (2012) 463–474.
[35] G. Sun, Z. Zhang, Mechanical properties of melamine-formaldehyde microcapsules, J. Microencapsul. 18 (5) (2001) 593–602.
[36] A. Gray, S. Egan, S. Bakalis, Z. Zhang, Determination of microcapsule physicochemical, structural, and mechanical properties, Particuology 24 (2016) 32–43.
[37] C.C.E. Akoh, Lipid-Based Emulsions and Emulsifiers, Fourth Edition (4th Ed.), CRC Press, 2017.
[38] K.C. Powell, A. Chauhan, Interfacial tension and surface elasticity of Carbon Black (Cb) covered oil–water interface, Langmuir 30 (41) (2014) 12287–12296.
[39] M.L. Taboada, T. Heiden-Hecht, M. Brückner-Gühmann, H.P. Karbstein, S. Drusch, V. Gaukel, Spray drying of emulsions: influence of the emulsifier system on changes in oil droplet size during the drying step, J. Food Process. Preserv. 45, (9) (2021) e15753.
[40] L. Bai, S. Huan, W. Xiang, L. Liu, Y. Yang, R.W.N. Nugroho, Y. Fan, O.J. Rojas, Self-assembled networks of short and long chitin nanoparticles for oil/water interfacial Superstabilization, ACS Sustain. Chem. Eng. 7 (7) (2019) 6497–6511.
[41] N. Gao, Y. Yan, Characterisation of surface wettability based on nanoparticles, Nanoscale 4 (7) (2012) 2202–2218.
[42] S. Asare-Asher, J.N. Connor, R. Sedev, Elasticity of liquid marbles, J. Colloid Interface Sci. 449 (2015) 341–346.
[43] D.S. Frost, J.J. Schoepf, E.M. Nofen, L.L. Dai, Understanding droplet bridging in ionic liquid-based Pickering emulsions, J. Colloid Interface Sci. 383 (1) (2012) 103–109.
[44] J. Xiao, X. Lu, Q. Huang, Double emulsion derived from Kafirin nanoparticles stabilized Pickering emulsion: fabrication, microstructure, stability and in vitro digestion profile, Food Hydrocoll. 62 (2017) 230–238.
[45] T. Tadros, P. Izquierdo, J. Esquena, C. Solans, Formation and stability of Nano-emulsions, Adv. Colloid Interf. Sci. 108-109 (2004) 303–318.
[46] A. Koocheki, R. Kadkhodaee, S.A. Mortazavi, F. Shahidi, A.R. Taherian, Influence of Alyssum Homolocarpum seed gum on the stability and flow properties of O/W emulsion prepared by high intensity ultrasound, Food Hydrocoll. 23 (8) (2009) 2416–2424.
[47] S.E. Friberg, Emulsion Stability, in: J. Sjöblom (Ed.), Emulsions - A Fundamental and Practical Approach, Springer, Dordrecht, 1992.
[48] C. Kai-Lai, W. De-Yong, Q. Tian-Peng, T. Jun, W. Hui-Hua, Physical and numerical simulation of the coalescence of liquid inclusion particles in molten steel, Chin. J. Eng. 41 (10) (2019) 1280.
[49] S.H. Mohd Taib, S.S. Abd Gani, M.Z. Ab Rahman, M. Basri, A. Ismail, R. Shamsudin, Formulation and process optimizations of nano-cosmeceuticals containing purified swiftlet Nest, RSC Adv. 5 (53) (2015) 42322–42328.
[50] K.L. Thompson, C.J. Mable, J.A. Lane, M.J. Derry, L.A. Fielding, S.P. Armes, Preparation of pickering double emulsions using block copolymer worms, Langmuir 31 (14) (2015) 4137–4144.
[51] X. Wang, W. Zhou, J. Cao, W. Liu, S. Zhu, Preparation of Core–Shell Caco3 capsules via pickering emulsion templates, J. Colloid Interface Sci. 372 (1) (2012) 24–31.
[52] A.R. Patel, C. Remijn, A.-I.M. Cabero, P.C.M. Heussen, J.W.M.S. ten Hoorn, K. P. Velikov, Novel all-natural microcapsules from gelatin and shellac for biorelated applications, Adv. Funct. Mater. 23 (37) (2013) 4710–4718.
[53] L.A. Gower, D.A. Tirrell, Calcium carbonate films and helices grown in solutions of poly(aspartate), J. Cryst. Growth 191 (1) (1998) 153–160.
[54] M. Huang, Y. Wang, Synthesis of calcium phosphate microcapsules using yeast-based biotemplate, J. Mater. Chem. 22 (2) (2012) 626–630.
[55] R.V. Bell, L.A. Rochford, R.T.M. de Rosales, M. Stevens, J.V.M. Weaver, S.A.F. Bon, Fabrication of calcium phosphate microcapsules using emulsion droplets stabilized with branched copolymers as templates, J. Mater. Chem. B 3 (27) (2015) 5544–5552.
[56] Z. Dong, L. Feng, Y. Hao, M. Chen, M. Gao, Y. Chao, H. Zhao, W. Zhu, J. Liu, C. Liang, Q. Zhang, Z. Liu, Synthesis of hollow biomineralized Caco3–polydopamine nanoparticles for multimodal imaging-guided cancer photodynamic therapy with reduced skin photosensitivity, J. Am. Chem. Soc. 140 (6) (2018) 2165–2178.
[57] Y. Wang, S. Zhang, D.S.W. Benoit, Degradable poly(ethylene glycol) (peg)-based hydrogels for spatiotemporal control of Sirna/nanoparticle delivery, J. Control. Release 287 (2018) 58–66.
[58] C. Dingels, H. Frey, From biocompatible to biodegradable: poly(ethylene glycol)S with predetermined breaking points, in: V. Percec (Ed.), Hierarchical Macromolecular Structures: 60 Years after the Staudinger Nobel Prize Ii, Springer International Publishing, Cham, 2013, pp. 167–190.
[59] M.A. Jumat, P. Chevallier, D. Mantovani, S. Saidin, Everolimus immobilisation using Polydopamine intermediate layer on poly(L-lactic acid)/poly(D-lactic acid) scaffold for sustainable anti-proliferative drug release, Mater. Today Commun. 31 (2022) 103720.
[60] X. Wang, B. Jin, X. Lin, In-situ Ftir spectroelectrochemical study of dopamine at a glassy carbon electrode in a neutral solution, Anal. Sci. 18 (8) (2002) 931–933.
[61] L.L. Richardson, C. Aguilar, K.H. Nealson, Manganese oxidation in Ph and O2 microenvironments produced by phytoplankton1,2, Limnol. Oceanogr. 33 (3) (1988) 352–363.
[62] Y. Liu, K. Ai, L. Lu, Polydopamine and its derivative materials: synthesis and promising applications in energy, environmental, and biomedical fields, Chem. Rev. 114 (9) (2014) 5057–5115.
[63] Z. Zhou, B. Zheng, Y. Gu, C. Shen, J. Wen, Z. Meng, S. Chen, J. Ou, A. Qin, New approach for improving anticorrosion and biocompatibility of magnesium alloys via polydopamine intermediate layer-induced hydroxyapatite coating, Surf. Interf. 19 (2020) 100501.
[64] F.K. Yang, B. Zhao, Adhesion properties of self-polymerized dopamine thin film, Open Surf. Sci. J. 3 (2011) 115–122.
[65] G. Yuan, X. Chen, X. Li, Q. Liang, G. Miao, B. Yuan, The synthesis of calcium carbonate microparticles with multiple morphologies through self-assembly method, Powder Technol. 284 (2015) 253–256.
[66] N.H. de Leeuw, S.C. Parker, Surface structure and morphology of calcium carbonate polymorphs calcite, aragonite, and vaterite: an atomistic approach, J. Phys. Chem. B 102 (16) (1998) 2914–2922.
[67] Q. Li, L. Dong, W. Deng, Q. Zhu, Y. Liu, C. Xiong, Solvent-free fluids based on rhombohedral nanoparticles of calcium carbonate, J. Am. Chem. Soc. 131 (26) (2009) 9148–9149.
[68] H. Tong, W. Ma, L. Wang, P. Wan, J. Hu, L. Cao, Control over the crystal phase, shape, size and aggregation of calcium carbonate via a L-aspartic acid inducing process, Biomaterials 25 (17) (2004) 3923–3929.
[69] Y. Long, K. Song, D. York, Z. Zhang, J.A. Preece, Engineering the mechanical and physical properties of organic–inorganic composite microcapsules, Colloids Surf. A Physicochem. Eng. Asp. 433 (2013) 30–36.

[70] J. Smets, A. Pintens, L. Orlandini, P.D. Sands, S.J. Guinebretiere, Benefit Agent-Containing Delivery Particle, US2015/0099680 A1, 2015.
[71] Y. Long, K. Song, D. York, Z. Zhang, J.A. Preece, Composite microcapsules with enhanced mechanical stability and reduced active ingredient leakage, Particuology 26 (2016) 40–46.
[72] Z. Zhang, R. Saunders, C.R. Thomas, Mechanical strength of single microcapsules determined by a novel micromanipulation technique, J. Microencapsul. 16 (1) (1999) 117–124.
[73] A.L. White, H.A. Javier, S. Withey, S.R. Biggs, S. Rose, S.G. Puttick, A.K. Whittaker, Deposition of non-porous calcium phosphate shells onto liquid filled microcapsules, J. Colloid Interface Sci. 609 (2022) 575–583.
[74] A.L. White, C. Langton, M.-L. Wille, J. Hitchcock, O.J. Cayre, S. Biggs, I. Blakey, A. K. Whittaker, S. Rose, S. Puttick, Ultrasound-triggered release from metal Shell microcapsules, J. Colloid Interface Sci. 554 (2019) 444–452.
[75] J. Hu, X. Zhang, J. Qu, Y. Wen, W. Sun, Synthesis, characterizations and mechanical properties of microcapsules with dual Shell of polyurethane (Pu)/melamine formaldehyde (mf): effect of different chain extenders, Ind. Eng. Chem. Res. 57 (10) (2018) 3591–3601.
[76] S. Liu, Understanding Molecular Interactions to Enhance Deposition of Perfume Microcapsules on Fabric Surfaces, PhD Thesis, University of Birmingham, Birmingham, UK, 2018.
[77] Y. He, J. Bowen, J.W. Andrews, M. Liu, J. Smets, Z. Zhang, Adhesion of perfume-filled microcapsules to model fabric surfaces, J. Microencapsul. 31 (5) (2014) 430–439.
[78] M. Liu, Understanding the Mechanical Strength of Microcapsules and their Adhesion on Fabric Surfaces,, PhD Thesis, University of Birmingham, Birmingham, UK, 2010.